Cell

A CXCL1 Paracrine Network Links Cancer Chemoresistance and Metastasis

Swarnali Acharyya,[1] Thordur Oskarsson,[1,9] Sakari Vanharanta,[1] Srinivas Malladi,[1] Juliet Kim,[1] Patrick G. Morris,[2] Katia Manova-Todorova,[3] Margaret Leversha,[4] Nancy Hogg,[7] Venkatraman E. Seshan,[6] Larry Norton,[2] Edi Brogi,[5] and Joan Massagué[1,8,*]

[1]Cancer Biology and Genetics Program
[2]Department of Medicine
[3]Molecular Cytology Core Facility
[4]Molecular Cytogenetics Core Facility
[5]Department of Pathology
[6]Department of Epidemiology and Biostatistics
Memorial Sloan-Kettering Cancer Center, New York, NY 10065, USA
[7]Leukocyte Adhesion Laboratory, Cancer research UK London Research Institute, London WC2A 3PX, UK
[8]Howard Hughes Medical Institute, Chevy Chase, MD 21205, USA
[9]Present Address: Heidelberg Institute for Stem Cell Technology and Experimental Medicine (HI-STEM), Im Neuenheimer Feld 280, 69120 Heidelberg, Germany
*Correspondence: massaguj@mskcc.org
DOI 10.1016/j.cell.2012.04.042

SUMMARY

Metastasis and chemoresistance in cancer are linked phenomena, but the molecular basis for this link is unknown. We uncovered a network of paracrine signals between carcinoma, myeloid, and endothelial cells that drives both processes in breast cancer. Cancer cells that overexpress CXCL1 and 2 by transcriptional hyperactivation or 4q21 amplification are primed for survival in metastatic sites. CXCL1/2 attract $CD11b^{+}Gr1^{+}$ myeloid cells into the tumor, which produce chemokines including S100A8/9 that enhance cancer cell survival. Although chemotherapeutic agents kill cancer cells, these treatments trigger a parallel stromal reaction leading to TNF-α production by endothelial and other stromal cells. TNF-α via NF-kB heightens the CXCL1/2 expression in cancer cells, thus amplifying the CXCL1/2-S100A8/9 loop and causing chemoresistance. CXCR2 blockers break this cycle, augmenting the efficacy of chemotherapy against breast tumors and particularly against metastasis. This network of endothelial-carcinoma-myeloid signaling interactions provides a mechanism linking chemoresistance and metastasis, with opportunities for intervention.

INTRODUCTION

Breast cancer remains the most common malignant disease in women, with one million new cases diagnosed worldwide per year, causing 400,000 deaths (Gonzalez-Angulo et al., 2007). The vast majority of these deaths are due to metastatic disease. Although the 5 year disease-free survival rate is 89% in patients with well-treated localized breast cancer, the appearance of metastatic disease is almost always a harbinger of eventual cancer mortality. The median survival of breast cancer patients with distant metastasis is between one and two years, and only a quarter of such patients survive 5 or more years from diagnosis of metastases (Jones, 2008).

The two established forms of systemic therapy for metastatic disease are hormonal treatments for hormone-dependent (estrogen and/or progesterone receptor positive) cases and cytotoxic chemotherapy for cases without hormone receptors. Hormone-dependent breast cancers frequently become refractory to initially effective hormonal treatments, thus eventually requiring chemotherapy as well. Trastuzumab, an antibody to the extracellular domain of the receptor c-erbB2/HER2, often augments the chemotherapy effect in cases overexpressing this gene (Pegram et al., 2004). Although tumor shrinkage is commonly accomplished on initial use of chemotherapy, the eventual emergence of tumor regrowth in the original as well as in new sites is common (Jones, 2008). On developing progressive disease after initial chemotherapy, different chemotherapy drugs are usually offered to patients, but the odds of response to subsequent administrations of chemotherapy decline with each episode of response and progression. Ultimately, pan-resistance occurs, which in association with the progression of metastatic spread, an almost universally linked process, is the cause of death (Gonzalez-Angulo et al., 2007).

Drug resistance in cancer can be cell-intrinsic (Poulikakos and Rosen, 2011) or a combination of host and tumor mediated pathways (Bergers and Hanahan, 2008; Ebos et al., 2009). In the case of chemotherapeutic agents, resistance develops because of both pre-established intrinsic mechanisms as well as those acquired de novo during the course of the treatment (Gonzalez-Angulo et al., 2007). Recent evidence points to tumor microenvironment components as potential participants in the generation of chemoresistance (Denardo et al., 2011; Gilbert

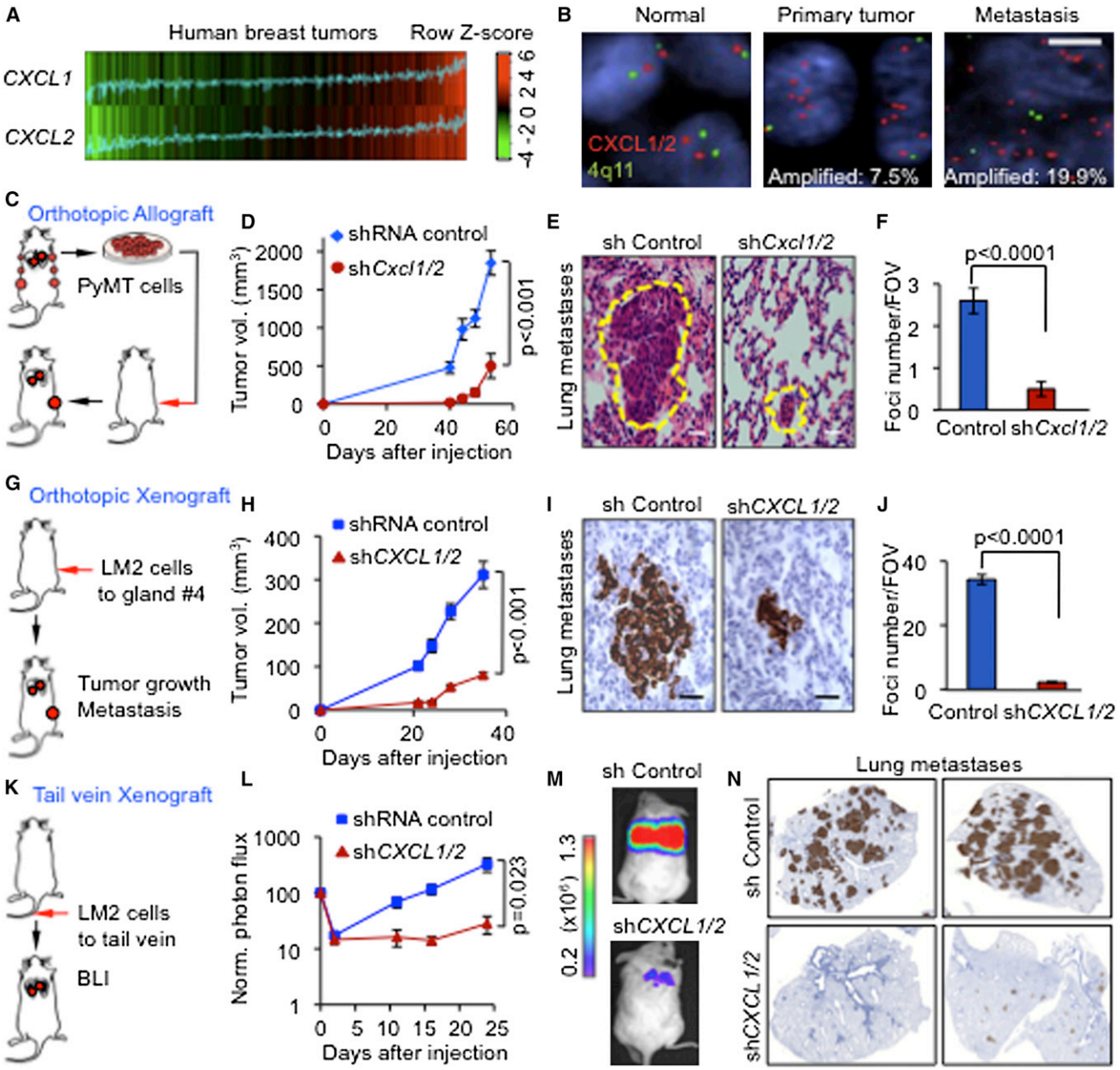

Figure 1. CXCL1/2 Mediate Mammary Tumor Growth and Lung Metastasis

(A) *CXCL1* and *CXCL2* expression in 615 primary breast cancers based on microarray gene expression data sets. Correlation between the two genes was determined by Pearson's correlation coefficient (n = 615, r = 0.53, $p < 2.2 \times 10^{-16}$). p value was determined by Student's t test.

(B) Breast cancer tissue microarray (TMA) samples composed of normal breast tissue, primary breast tumors and metastases (LN from lymph node and lung metastases) from patients analyzed by FISH. Signals in green correspond to 4q centromeric reference probe and signals in red correspond to *CXCL1/2* probes. Scale bar, 2.5 μm.

(C) Schematic representation of breast cancer progression in orthotopic allograft model. PyMT mammary cancer cells were isolated from MMTV-PyMT mammary tumors, transduced with shRNA control or sh*Cxcl1/2*, and transplanted into syngeneic mice.

(D) Growth curves of tumors from control and sh*Cxcl1/2* PyMT-F cells. Data are averages ± SEM; n = 6 mice per group.

(E) Spontaneous lung metastasis determined by H&E staining of lung sections at week 9 after tumor inoculation at endpoint. Scale bars,10 μm.

(F) Quantitation of lung metastasis determined by automated counting of foci per field of view (FOV). Data are averages ± SEM; n = 6 mice per group. p values were determined by Student's t test.

(G) Schematic representation of breast cancer progression in orthotopic xenograft model. LM2 metastatic breast cancer cells were implanted into immunodeficient NOD-SCID mice. Mammary tumor growth and lung metastasis were determined.

(H) Growth curves of tumors from LM2 cells transduced with control or *CXCL1/2* shRNA. Data are averages ± SEM. Control, n = 13, sh*CXCL1/2*, n = 7.

(I) Representative histology images of spontaneous lung metastasis detected by vimentin immunostaining. Scale bars, 60 μm.

and Hemann, 2010; Roodhart et al., 2011; Shaked et al., 2008; Shree et al., 2011). However, an integrated understanding of acquired drug resistance in the context of inputs from tumor and its microenvironment is lacking. Such insights could be critical for designing more effective therapies to overcome resistance and improve outcome from a palliative to curative clinical response in cancer.

Clinically as well as biologically, metastasis is intricately linked with resistance to chemotherapy (Hu et al., 2009; Morris et al., 2009). Biologically, less than 0.1% of the circulating cancer cells are estimated to withstand the harsh stresses of infiltrating and colonizing distant metastatic sites (Weiss, 2000). Similarly, a very small fraction of cells exposed to genotoxic stress can survive and outgrow under repeated cycles of chemotherapy.

This combined clinical and biological problem prompted us to ask whether both metastatic and chemotherapeutic stresses might select for cancer cells with a common set of survival advantage mechanisms. We uncovered a paracrine network, with the chemokines CXCL1 and 2 at its core, that mediates lung metastasis and chemoresistance in breast cancer. We identified the signals from cancer cells that trigger this paracrine cascade, the specific stromal cell types that respond to these signals, the cancer cell survival factors delivered by the stromal cells, and the survival response of cancer cells to these stromal factors. We delineated how chemotherapy triggers a parallel reaction in the stroma and amplifies this paracrine network making therapy less effective. Blocking this axis with CXCL1/2 receptor inhibitors in combination with chemotherapy markedly reduced metastatic burden in preclinical models, addressing the key problem of why chemotherapeutic treatments fail and lead to relapse.

RESULTS

CXCL1/2 Mediate Mammary Tumor Growth and Lung Metastasis

Several observations provided a rationale to explore the potential role of *CXCL1/2* in breast cancer progression and metastatic recurrence to the lungs. *CXCL1* emerged among a set of genes whose expression is associated with lung relapse in breast tumors, including tumors that had not been exposed to prior chemotherapy (Minn et al., 2007; Minn et al., 2005), and as a gene that increases the aggressiveness of circulating breast tumor cells (Kim et al., 2009). *CXCL1* and *2* are 90% identical by amino acid sequence and signal through the same receptor CXCR2 (Balkwill, 2004). Indeed, *CXCL1* and *CXCL2* showed a similar expression pattern in a combined cohort of 615 primary breast cancers (Figure 1A). Copy number alterations at 4q21 occur in breast cancer (Beroukhim et al., 2010) and engulf 15 genes in the amplification peak, including *CXCL1-8*. Fluorescence in situ hybridization (FISH) of human tissue samples showed that *CXCL1* and *CXCL2* were amplified in 7.5% of primary breast tumors and in 19.9% of metastases (Figures 1B and S1A available online). These results suggested that increased copy number contributes to the higher *CXCL1/2* expression in invasive breast tumors and metastases. Additionally, high expression of *CXCL1* in breast tumors without gene amplification is also possible (Bièche et al., 2007).

Prompted by these findings we investigated the role of CXCL1 and 2 in breast cancer. We utilized two independent experimental systems. First, a syngeneic transplant system with cell lines derived from mammary tumors driven by a polyoma middle T transgene in two different MMTV-PyMT mouse strains, FVB/N (PyMT-F for short) and C57BL/6 (PyMT-B) (Stewart and Abrams, 2007). Second, a xenograft model to orthotopically implant LM2-4175 lung metastatic cells (LM2 for short) was derived from the MDA-MB-231 human breast cancer cell line (Minn et al., 2005). LM2 cells showed upregulation of *CXCL1/2* compared to the parental line (Figure S1B). PyMT-F and LM2 cells grew aggressively in the mammary fat pad and metastasized to the lungs. Knockdown of *CXCL1* and *2* using two independent shRNA hairpins (Figures S1C and S1D) significantly reduced mammary tumor growth in all three models (Figures 1C, 1D, 1G, and 1H, S1E, and S1F) This decrease was associated with reduced metastasis in the lungs (Figures 1E, 1F, 1I, 1J, and S1G). Similar results were obtained upon size-matching the knockdown tumors to controls (Figures S1H and S1I). Furthermore, lung colonization assays by tail-vein injection of LM2 cells confirmed that the effect of CXCL1/2 depletion on metastasis is not solely a consequence of decreased tumor burden (Figures 1K–1N). Interestingly, among other CXCR2 ligands that we tested, CXCL3 knockdown in LM2 cells contributed to tumor growth but not metastasis (Figures S1K–S1M). We concluded that CXCL1/2 play a prominent role in breast cancer progression and metastasis.

CXCL1/2 Recruit Myeloid Cells to Mammary Tumors

Reduction in CXCL1/2 levels in the LM2 xenograft and PyMT transplantation models was associated with a significant increase in apoptosis in the tumors (Figures 2A and 2B). However, CXCL1/2 knockdown was not accompanied by any visible changes in apoptosis in vitro or in angiogenesis and cell proliferation rates in tumors (Figures S2A–S2E). The function of CXCL1/2 is primarily mediated by binding to the G protein coupled receptors, CXCR2 and, in some instances, CXCR1 and DARC (Balkwill, 2004). Compared to the high levels of

(J) Quantitation of lung metastatic burden determined by automated counting of number of foci per FOV. Shown are averages ± SEM; n = 5 mice per group. p values was determined by Student's t test.

(K) Schematic representation of lung colonization assay in xenograft model. Luciferase labeled MDA231-LM2 cells transduced with control or sh*CXCL1/2* were injected intravenously and monitored over time by noninvasive BLI.

(L) BLI quantification of lung colonization ability of control or sh*CXCL1/2* LM2 cells. Data are averages ± SEM; n = 7 per group. p values were determined by Student's t test.

(M) Representative BLI images of mice with lung metastasis.

(N) Cancer cells in the lungs stained for vimentin expression.

See also Figure S1.

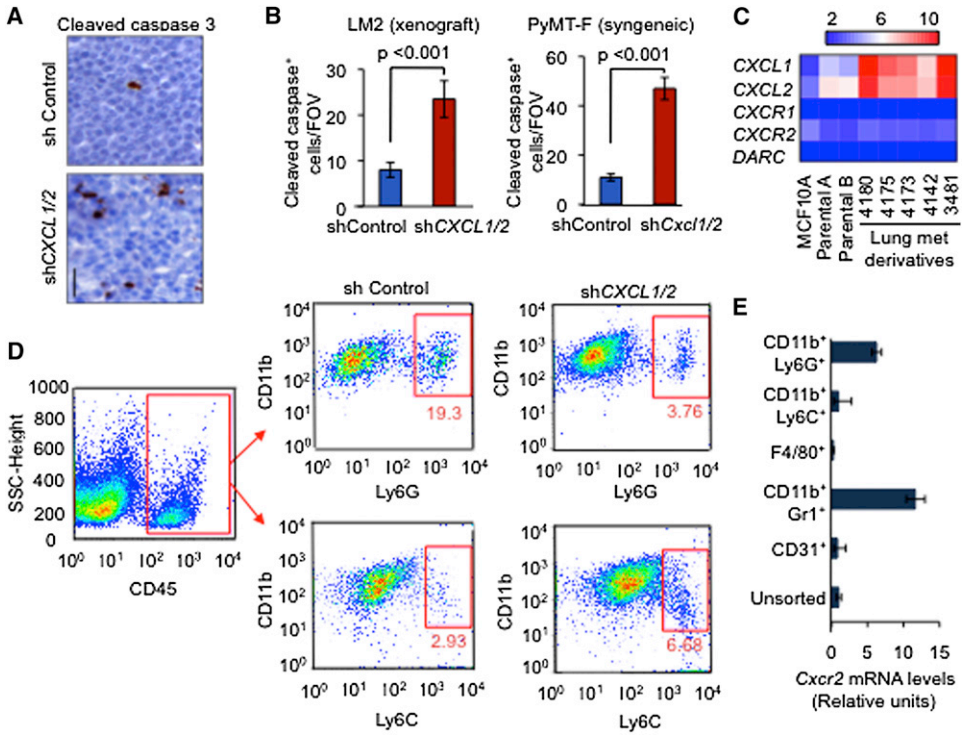

Figure 2. Carcinoma-Derived CXCL1/2 Supports Cancer Cell Survival and Recruit Granulocytic Myeloid Cells to Tumors

(A and B) Representative images and quantification of apoptosis in mammary tumors analyzed by cleaved caspase-3 staining. Mouse mammary glands were injected with LM2 cells (A and B) or PyMT-F cells (B) expressing shRNA control or sh*CXCL1/2* and analyzed at endpoint (LM2, 6 weeks; PyMT-F, 9 weeks after tumor implantation). Scale bar, 30 μm. Data are averages ± SEM; n = 4 mice per group. p values were calculated by Student's t test.

(C) Expression of the indicated genes from microarray gene expression analysis in nontumor human mammary epithelial cell line MCF10A, parental MDA-MB-231 breast cancer cells and lung metastatic lines derived from MDA-MB-231 (Minn et al., 2005).

(D) Flow cytometric analysis of recruited myeloid cells in tumors formed by LM2 cells transduced with either control shRNA or sh*CXCL1/2* at 5 weeks after tumor inoculation. A representative gating is shown. Numbers indicate either $CD11b^+Ly6G^+$ or $CD11b^+Ly6C^+$ cells in the quadrant expressed as percentages of total $CD45^+$ leukocytes from the same tumor. Results are representative of three independent experiments (n = 3).

(E) Expression of *Cxcr2* receptor in sorted subpopulations of LM2 tumors determined by qRT-PCR. Error bars represent 95% confidence interval for qRT-PCR analysis. Data are representative of two independent experiments.

See also Figure S2 and Tables S1 and S2.

CXCL1/2 expression in lung metastatic cell lines, the expression of CXCR1, CXCR2, and DARC was negligibly low both at the RNA and protein levels (Figure 2C and Figure S2F and Müller et al., 2001). Based on these results, we postulated that CXCL1/2 mediates tumor cell survival via paracrine mechanisms.

CXCR2 receptor is expressed by several stromal cell types such as endothelial and myeloid cells (Murdoch et al., 2008). Using a combination of immunostaining and FACS, we did a comprehensive analysis of major cell types in the tumor microenvironment whose abundance changed upon *CXCL1/2* knockdown in the LM2 xenograft and PyMT-F transplant models. A significant reduction in $CD11b^+Gr1^+$ myeloid cells was observed in *CXCL1/2* knockdown tumors in both models (Figures S2G and S2H). Myeloid-derived suppressor cells (MDSC) represent a heterogeneous group including precursors for neutrophils and monocytes that express both CD11b and Gr1 (Gabrilovich and Nagaraj, 2009). $Gr1^+$ in mice includes cells that express the macrophage marker Ly6C and cells that express the neutrophil marker Ly6G (Ostrand-Rosenberg and Sinha, 2009). Detailed characterization of the myeloid cells showed a decrease in the $CD11b^+Ly6G^+$ granulocytic MDSC population in CXCL1/2 knockdown tumors compared to controls (Figures 2D and S2I). No appreciable decrease was observed in the $CD11b^+Ly6C^+$, $F4/80^+$ macrophages, SMA^+ myofibroblast, $Ter119^+$ erythroid cells, or endothelial cells in the CXCL1/2 depleted tumors (Figures S2J–S2P, Table S1, and data not shown). In line with our hypothesis, $CD11b^+Gr1^+$ cells and specifically the $CD11b^+Ly6G^+$ subpopulation expressed CXCR2 (Figures 2E and S2Q). Within the recruited $CD11b^+Ly6G^+$ population in the PyMT immunocompetent transplant tumors, 6%, 12%, and 25% of the cells expressed CD80, F4/80, and Sca1, respectively, and a minority expressed CD86, CD117, IL4Rα, VEGFR1, and CD34 (Table S2). Sca1, a marker of the hematopoietic stem cells, was expressed in $CD11b^+Ly6G^+$ populations, indicating potential progenitor-like phenotype of the tumor granulocytic cells recruited by CXCL1/2 (Table S2).

Interestingly, a reduction both in monocytic $CD11b^+Ly6C^+$ and granulocytic $CD11b^+Ly6G^+$ cells occurred in the lungs of mice bearing CXCL1/2 depleted tumors with minimal changes in the number of $F4/80^+$ macrophages (Figures S2R–S2T). Compared

to the myeloid components, lymphocytic cells represented a minority of leukocytes infiltrated in the immunocompetent PyMT transplanted tumors (Table S1). CXCL1/2 depleted tumors showed a decrease in $CD4^+$ and $CD8^+$ lymphocytes, no major change in $\gamma\delta$-TCR^+ and $CD25^+$ T regulatory cells, and moderate increases in $B220^+$ lymphocyte and $CD49b^+$ NK cell numbers (Table S1). Given the low numbers and small differences within lymphocytic populations in the tumors, we chose to focus on $CD11b^+Gr1^+$ cells that are the predominant cell type recruited by CXCL1/2 in the tumor microenvironment in multiple models.

CXCL1/2 Promote Metastasis through Myeloid-Cell-Derived S100A8/9

Results from our functional analysis suggested that myeloid cell types recruited by CXCL1/2 might provide paracrine factors that support the survival of cancer cells. To identify such factors, we analyzed human breast tumor gene expression data sets for genes that are expressed in association with *CXCL1* (Figure 3A). Focusing on paracrine mediators, we filtered genes encoding cell surface and secreted products. Analysis of 615 breast tumors from three independent data sets yielded 43 such genes that correlated with *CXCL1* with a coefficient > 0.3 (Figure 3A and Table S3). These genes showed a predominance of chemokines (40%) and cytokines (21%). Similar analysis of a data set generated from 67 metastases from breast cancer patients showed a 61% overlap in *CXCL1*-associated genes between primary breast tumors and metastases (Figure 3B and Tables S3 and S4).

To identify cancer cell survival factors derived from the recruited myeloid cells, we identified candidates that are abundantly expressed in tumor-derived $CD11b^+Gr1^+$ cells and are not of epithelial origin (Figures 3C and 3D and Figure S3A). *S100A8* and *A9* fulfilled these criteria. S100A8/9 are low molecular weight calcium binding proteins that are associated with chronic inflammation and cancer (Gebhardt et al., 2006). S100A8/9 bind to Toll-like receptor 4 (TLR4) and RAGE (receptor for advanced glycation end products), which activate diverse signaling cascades (Gebhardt et al., 2006; Vogl et al., 2007). Both TLR4 and RAGE are expressed in breast cancer cells (Bos et al., 2009; Hsieh et al., 2003).

To determine whether myeloid S100A8/9 stimulate tumor growth and metastatic phenotype of breast cancer cells, we isolated bone marrow cells from $S100A9^{+/+}$ and $S100A9^{-/-}$ mice (Hobbs et al., 2003) and transplanted them into irradiated immunocompromised mice. In addition to lacking S100A9, $S100a9^{-/-}$ bone-marrow-derived cells fail to express S100A8, which is the heterodimeric partner of S100A9 (Figure S3B) (Hobbs et al., 2003). After confirming successful engraftment of $S100a9^{+/+}$ or $S100a9^{-/-}$ bone marrow with an efficiency of > 98% (Figure S3C), we implanted LM2 cancer cells in the mammary fat pads of these mice. Mammary tumor growth and lung metastasis were significantly reduced in mice transplanted with $S100a9^{-/-}$ bone marrow compared to the $S100a9^{+/+}$ counterpart (Figures 3E–3G).

To confirm these results in a different system, we stably reduced the expression of *S100a8/9* in MPRO, a murine bone-marrow-derived promyelocytic cell line (Figure S3D) that expresses both CD11b and Gr1 (Tsai and Collins, 1993). Coinjection of wild-type MPRO cells with LM2 cancer cells enhanced mammary tumor growth and lung metastasis, an effect that was significantly blunted by *S100a8/9* knockdown in the MPRO cells (Figures S3E and S3F). Furthermore, the enforced expression of *S100a8/9* in LM2 cells (Figures S3G and S3H) rescued the *CXCL1/2* knockdown phenotype of reduced tumor growth and metastasis (Figures 3H, 3I, and S3I). Together, these results suggest that S100A8/9 mediate the prometastatic effect of CXCL1/2 in our models.

Based on the accumulating evidence of a role of S100A8/9 in breast cancer metastasis in animal models, we sought evidence for this link in clinical samples. We immunostained tissue microarrays composed of lung metastasis samples from breast cancer patients with an antibody recognizing human S100A8/9 (Figure 3J). Kaplan Meier analysis showed that patients with high S100A8/9 in the metastatic nodules had a significantly shorter overall survival compared to low S100A8/9 (p value = 0.01) (Figure 3K). Collectively our results suggest that CXCL1/2 from breast cancer cells recruit myeloid producers of S100A8/9, which in turn promote breast cancer metastasis.

S100A8/9 Promotes Breast Cancer Cell Survival under Chemotherapy

We investigated whether S100A8/9 in tumors are linked to enhanced cancer cell survival. Tumor-bearing mice transplanted with $S100a9^{-/-}$ bone marrow showed a marked increase in the number of apoptotic cells in the mammary tumors and the lung (Figure 4A). The requirement of S100A8/9 in cell survival was even more evident when tumor-bearing mice were treated with chemotherapeutic agents as an inducer of cell death (Figures 4B and 4C and S4A).

Similar numbers of $CD11b^+$ and $CD68^+$ myeloid cells were present in tumors and lung nodules from mice transplanted with either $S100a9^{-/-}$ or $S100a9^{+/+}$ bone marrow cells (Figure S4B and data not shown). This result ruled out the possibility that higher apoptotic rates in the $S100A9^{-/-}$ group were due to a defective accumulation of myeloid cells (Hiratsuka et al., 2008). Consistent with the survival advantage provided by S100A8/9 in vivo, coculture of cancer cells with bone-marrow-derived $CD11b^+Gr1^+$ cells protected cancer cells from doxorubicin-induced apoptosis (Figure 4D). However, this protection was more limited in coculture with $CD11b^+Gr1^+$ cells derived from $S100A9^{-/-}$ marrow (Figure 4D), confirming that the prosurvival properties of myeloid factors under stress chemotherapy conditions are partly due to S100A8/9.

Binding of S100A8/9 to receptors RAGE and TLR4 can activate diverse signaling cascades (Gebhardt et al., 2006; Ichikawa et al., 2011; Vogl et al., 2007). S100A8/9 addition only weakly activated NFκB in LM2 breast cancer cells and we detected no activation of the Akt or STAT3 pathways (Figure S4C and data not shown). Using blot arrays that detect phosphorylation of 46 different protein kinases, we found that S100A8/9 cause activation of ERK1/2, p38 MAPK, and p70S6K in LM2 cells (Figures 4E and S4D), as confirmed by immunoblotting (Figures S4E and S4F). Addition of an ERK1/2 inhibitor (FR180204) or a p70S6K inhibitor (PF4708671) abolished the chemo-protective effect of S100A8/9, whereas addition of a p38 inhibitor (SB203580) showed partial effect (Figure 4F), suggesting that

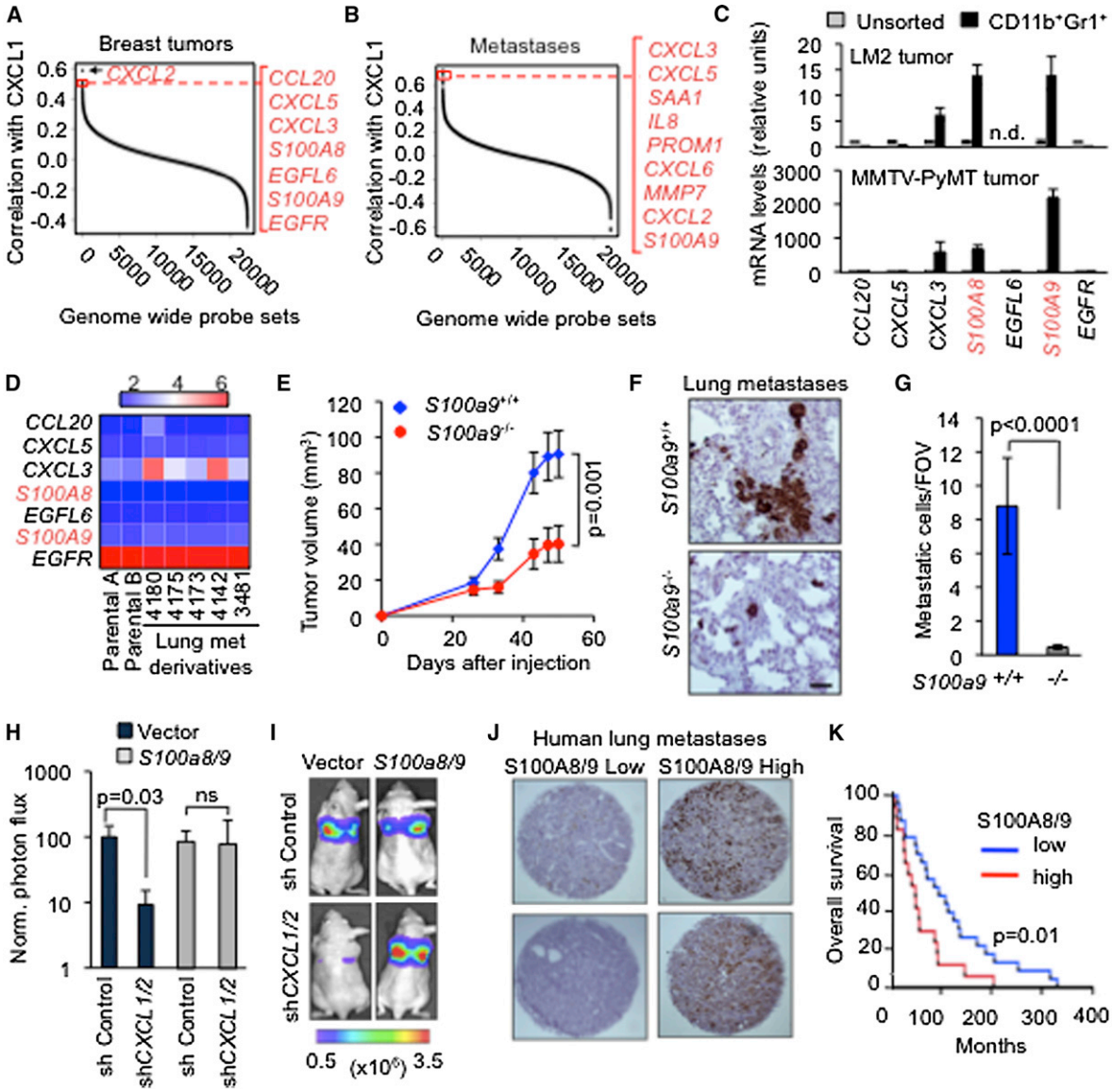

Figure 3. CXCL1/2 Promote Metastasis through Myeloid-Cell-Derived S100A8/9

(A and B) Gene ranking according to correlation with *CXCL1* expression. Expression data from breast cancer primary and metastases microarray data sets. Genes were filtered based on extracellular localization to identify paracrine mediators. The list on the right shows genes that correlate highest with *CXCL1*. Complete list of CXCL1 correlating genes in Tables S3 and S4.

(C) Expression of the top seven *CXCL1*-associated genes in (A) in the sorted CD11b^{+}Gr1^{+} cells compared to unsorted tumor determined by qRT-PCR analysis from LM2 breast cancer model and MMTV-PyMT autochthonous mammary cancer model. Error bars represent 95% confidence interval. Data are representative of two independent experiments.

(D) Expression of top seven *CXCL1*-associated genes in breast cancer cell lines based on microarray gene expression data.

(E) LM2 tumor growth curves in mice transplanted with either *S100a9*$^{+/+}$ or *S100a9*$^{-/-}$ bone marrow. Data points show averages ± SEM; n = 19 tumors per group. p value was determined by Student's t test.

(F and G) Representative images and quantitation of metastatic cells in lungs detected by vimentin immunohistochemistry at 60 days after inoculation of LM2 tumors, in mice that were transplanted with *S100a9*$^{+/+}$or *S100a9*$^{-/-}$ bone marrow. Scale bar, 60 μm. Data points show averages ± SEM; n = 4–6 mice per group. p value was determined by Student's t test.

(H and I) Lung colonization by LM2 cells transduced with control shRNA or sh*CXCL1/2*, with or without ectopic expression of *S100a8/9*. Lung colonization was assessed by noninvasive BLI at 4 weeks after tail-vein injection of the cells. (H) Normalized BLI quantification. (I) images represented by photon flux of lung colonization ability. Data are averages ± SEM; n = 4–6 per group. *ns*, not significant. p value was determined by two-tailed Wilcoxon rank-sum test.

(J) Representative TMA cores containing lung metastasis samples from breast cancer patients stained for total S100A8/9.

(K) Kaplan-Meier overall survival analysis on breast cancer patients classified by total S100A8/9 expression in lung metastasis (see J) n = 23 for S100A8/9 low group, n = 17 for S100A8/9 high group. p values were calculated by log-rank test.

See also Figure S3 and Tables S3 and S4.

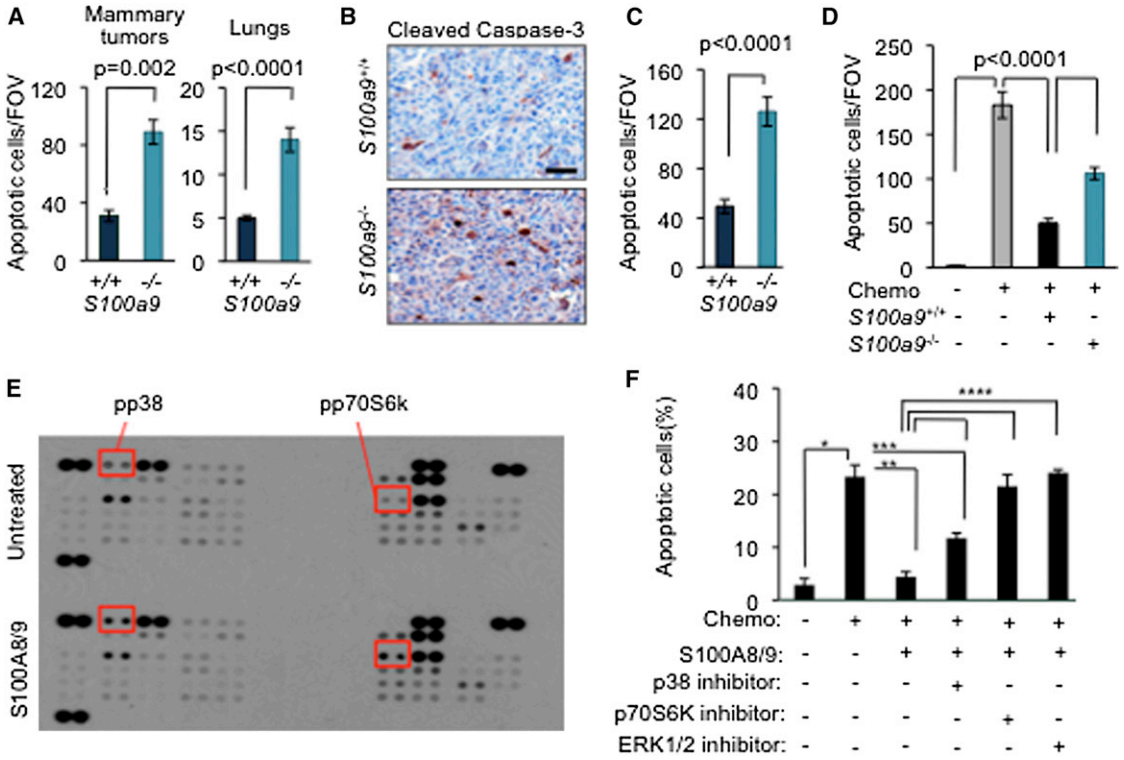

Figure 4. S100A8/9 Promotes Breast Cancer Cell Survival under Chemotherapy

(A) Quantitation of apoptosis by cleaved caspase-3 staining in tumors and TUNEL assay in lungs in mice transplanted with *S100a9*$^{+/+}$or *S100a9*$^{-/-}$ bone marrow at 60 days after LM2 tumor inoculation into the mammary fat pad. Data are averages ± SEM; n = 4–6 mice per group. p values were determined by Student's t test.

(B and C) Representative images and quantification of apoptosis by cleaved caspase 3 staining in LM2 tumors from mice transplanted with either *S100a9*$^{+/+}$or *S100a9*$^{-/-}$ bone marrow and subsequently treated with a combination of doxorubicin and cyclophosphamide chemotherapy (AC regimen, chemo) once weekly for 3 weeks. Scale bar, 32 μm. Data are averages ± SEM; n = 5–6 tumors per group. p values were determined by Student's t test.

(D) TUNEL analysis detecting apoptotic cancer cells in coculture assay. LM2 cancer cells were cultured alone or overnight in the presence of *S100a9*$^{+/+}$ or *S100a9*$^{-/-}$ bone marrow cells and subsequently treated with chemotherapeutic drug (Chemo), doxorubicin (0.8 μM). Data are average ± SEM of triplicates. p values determined by Student's t test.

(E) Screening of signaling pathways activated by S100A8/9 in LM2 metastatic cancer cells by probing human phosphokinase array with lysates from cells treated with either PBS or 10 μg/ml recombinant S100A8/9. Shorter exposure of the same blot shown in S4. Proteins showing increased phosphorylation upon S100A8/9 treatment are highlighted.

(F) TUNEL analysis detecting apoptotic cancer cells in coculture assay upon pharmacological inhibition of p38, p70S6K and ERK pathways in the presence of recombinant S100A8/9. LM2 cancer cells were pretreated with 10 μg/ml of S100A8/9 for 1 hr and subsequently treated with doxorubicin (0.8 μM, chemo) either alone or in the presence of 5 μM of p38 inhibitor SB203580 or 10 μM of p70S6K inhibitor PF4708671 or 10 μM of ERK inhibitor FR180204 for 16h. LM2 cells treated with saline were used as controls. Quantification of apoptosis was done by calculating the percentage of TUNEL^{+}/DAPI^{+} cells per FOV. Data are shown as average ± SEM from triplicates. * p = 0.004, ** p = 0.02, *** p = 0.04, ****p = 0.01. p values were determined by Student's t test.

See also Figure S4.

the ERK1/2 and p70S6K signaling mediate the prosurvival effect of S100A8/9 in metastatic cells.

The CXCL1/2–S100A8/9 Survival Axis Is Hyperactivated by Chemotherapy

Most patients who develop metastatic disease receive chemotherapy at some point in the management of their illness. Tumor shrinkage—partial or, less commonly, complete remissions—is usually accomplished, but these benefits are transient, and most patients eventually develop chemotherapy-resistant, widely disseminated cancer (Gonzalez-Angulo et al., 2007; Jones, 2008). We hypothesized that the CXCL1/2-S100A8/9 survival axis could nurture tumor cells under chemotherapeutic stress thereby selecting for aggressive metastatic progeny. To address this question, we treated mice bearing LM2 tumors with doxorubicin and cyclophosphamide (AC regimen), a commonly used chemotherapy combination in the clinic. MDA-MB-231, the parental breast cancer cell line from which LM2 was derived, was originally isolated from pleural effusion of a patient who was resistant to AC and 5-fluorouracil chemotherapy and had relapsed (Cailleau et al., 1974). Chemotherapy treatment of mice bearing LM2 tumors initially resulted in significant apoptosis and a concomitant delay in tumor growth (Figures 5A and 5B). However, after subsequent rounds of chemotherapy, tumors became refractory, as evidenced by a reduction in apoptosis and resumed tumor growth (Figures 5A and 5B).

To investigate the involvement of the CXCL1/2-S100A8/9 in cancer cell survival during chemotherapy challenge, we

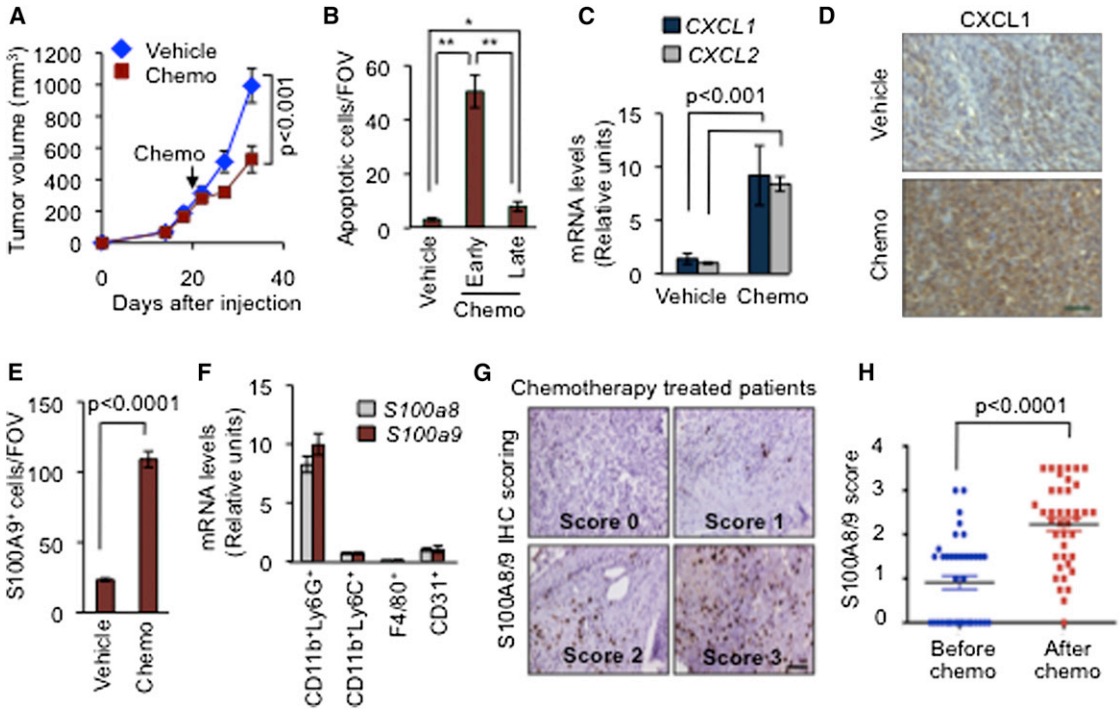

Figure 5. CXCL1/2 Paracrine Axis Is Hyperactivated upon Chemotherapy Treatment

(A) Tumor growth in mice treated with saline vehicle or a combination of doxorubicin and cyclophosphamide chemotherapy (AC chemo). The treatment was initiated once LM2 tumors reached 300 mm^3 and was repeated once weekly. Data represent averages ± SEM; n = 6–8 mice per group. p values were determined by Student's t test.

(B) Apoptosis determined by TUNEL staining in tumors treated with vehicle or AC chemotherapy for 3 days (early) or 8 days (late) both using the same treatment regimen. Data represent averages ± SEM; n = 3–5 mice per group. p values were calculated by Student's t test. *p = 0.02, **p < 0.0001.

(C) *CXCL1/2* expression in whole tumors harvested from mice treated with saline vehicle or AC chemotherapy for 8 days. Data represent averages ± SEM; n = 6–8 mice per group. p values were determined by Student's t test.

(D) Representative CXCL1 expression in whole tumors analyzed by immunohistochemistry harvested from mice treated with saline vehicle or AC chemotherapy (prolonged treatment) from two independent cohorts of three mice each. Scale bar, 70 μm.

(E) Quantitation of S100A9 positive cells in tumors from control and AC chemotherapy-treated mice (prolonged treatment). Data presented are average numbers of S100A9 positive cells per FOV ± SEM; n = 4–5 mice/group. Data representative of three independent experiments.

(F) Expression of *S100a8 and S100a9* in sorted subpopulations of LM2 tumors after chemotherapy treatment determined by qRT-PCR. Error bars represent 95% confidence interval. Data representative of two independent experiments.

(G) Immunohistochemical analysis of S100A8/9 in tumors from breast cancer patients before and after AC chemotherapy treatment. Representative images of scored S100A8/9 sections are shown. Scale bar, 60 μm.

(H) S100A8/9 expression score in paired patient tumor samples, before and after chemotherapy. Data represent expression score. n = 40. p values determined by Wilcoxon's paired test, comparing pre- and posttreatment levels from each patient.

See also Figure S5 and Table S5.

analyzed the expression of *CXCL1* and *CXCL2* in AC chemotherapy-treated tumors. AC-treated tumors significantly upregulated *CXCL1/2* expression (Figures 5C and 5D) and this effect was associated with increased recruitment of S100A9-expressing cells (Figure 5E) and $CD11b^+Ly6G^+$ granulocytic cells (Figure 5F). CXCL1/2 upregulation in the LM2 tumors was also observed with another commonly used chemotherapeutic agent, paclitaxel (Figure S5A). In addition to *CXCL1/2* and *S100A8/9*, the *CXCL1*-associated chemokine genes *CCL20* and *CXCL3* were also highly expressed in response to chemotherapy (Figure S5B). Although induction of CXCL chemokines occurs during chemotherapy-induced senescence (Coppé et al., 2008), there was no discernible increase in senescence in LM2 tumors upon AC chemotherapy treatment (Figures S5C and S5D). Together, these results suggest that chemotherapy activates a burst of paracrine factors including the cancer cell survival axis CXCL1/2-S100A8/9 that selects for cancer cells that can resist chemotherapy.

S100A8/9 Association with Resistance to Perioperative Chemotherapy

Neoadjuvant chemotherapy—the use of cytotoxic drugs prior to surgery for primary breast cancer—is an option for patients with operable disease. This has long been the standard approach for patients with locally advanced primary disease in an effort to shrink the tumor and thereby make complete tumor removal possible. Although these treatments usually cause tumor volume regression, some cases are chemotherapy-resistant de novo

(Gonzalez-Angulo et al., 2007). To address whether the CXCL1/2-S100A8/9 survival loop is activated in cancer patients with primary disease, we stained matched breast tumor sections from a cohort of patients before and after chemotherapy treatment. Consistent with our experimental models, a significant increase in S100A9-expressing cells was observed in breast cancers after chemotherapy treatment (Figures 5G and 5H and Table S5). In contrast, Fascin that is part of a lung metastasis gene signature (Minn et al., 2005) did not show the same trend upon chemotherapy treatment as S100A8/9 (Figure S5E), further confirming the specificity of the association of S100A8/9 with chemotherapy resistance.

Chemotherapy Induces TNF-α to Boost the CXCL1/2-S100A8/9 Axis

Hyperactivation of the CXCL-S100A8/A9 loop upon chemotherapy treatment prompted us to explore the mechanism behind the therapy-induced CXCL1/2 upregulation. In our experimental models, enhanced expression of CXCL1/2 in response to chemotherapy was not due to additional amplification of the locus as determined by FISH analysis (Figure S6A). Direct treatment of LM2 cells with the chemotherapeutic agents did not induce CXCL1/2 expression (Figure S6B and data not shown). However, LM2 tumor cells incubated with conditioned media from chemotherapy-treated primary endothelial cells or primary bone-marrow-derived cells showed a significant increase in CXCL1/2 expression (Figures 6A and S6B).

CXCL1/2 are target genes of the NFκB/STAT1 pathway (Amiri and Richmond, 2003). Among a panel of prototypical activators of the NFκB/STAT1 pathway that we assayed by qRT-PCR, *TNF-α* was strikingly induced in endothelial cells upon doxorubicin chemotherapy treatment (Figure 6B). Moreover, we observed a 10-fold increase in *TNF-α* expression in purified lung endothelial cells from LM2 tumor-bearing mice systemically treated with AC chemotherapy (Figures 6C and 6D). *TNF-α* induction in response to chemotherapy also occurred in smooth muscle and bone-marrow-derived cells (Figure 6E) suggesting that TNF-α release is a general response to chemotherapy in different stromal cell types. NFκB activation by TNF-α stimulated the expression of *CXCL1/2* in LM2 tumor cells, as determined with the use of NFκB pathway inhibitor (Nemo binding domain peptide or NBD) (Figure 6F). Thus, TNF-α from chemotherapy-activated stroma can boost the CXCL1/2-S100A8/9 loop. Treatment with anti-TNF-α antibody infliximab reduced recruitment of S100A9-expressing cells in chemotherapy-treated mammary tumors (Figures 6G and 6H). These tumors were formed with cell line CN34-LM1 derived from the pleural fluid of a stage IV breast cancer patient whose disease had progressed on therapy (Tavazoie et al., 2008). CN34-LM1 is more indolent than LM2 and allows for longer-term tumor growth experiments.

Consistent with our hypothesis, a significant increase in TNF-α immunostaining was observed in patient samples after neoadjuvant AC chemotherapy treatment (Figures 6I–6K) and in LM2 mammary tumors in mice treated with AC chemotherapy (Figure S6C). Importantly, histopathological analysis revealed that cells from the tumor microenvironment, specifically lymphatic and blood vessels and fibroblast-rich stroma, showed strong TNF-α staining after chemotherapy (Figures 6J and S6D).

Blocking CXCL1 Signaling Increases the Effectiveness of Chemotherapy

Our findings suggest that a self-defeating consequence of at least some chemotherapy drugs is the release of potent proinflammatory cytokines such as TNF-α from stromal sources. Such proinflammatory bursts can boost the CXCL1/2-S100A8/9 survival axis and facilitates the expansion of chemoresistant breast cancer cells. These results presented us with an option of targeting the tumor microenvironment in order to sensitize breast cancer cells to chemotherapy and to the stress of invading and colonizing distant tissues. Therefore, we utilized antagonists of CXCR2, the primary receptor for CXCL1/2, because derivatives of these pharmacological inhibitors are in clinical trials for chronic inflammatory diseases and show no major toxicity with long-term usage (Chapman et al., 2009). Furthermore, targeting the immune microenvironment would be an attractive option because of the potentially low selective pressure for mutations and epigenetic changes on the stroma compared to the cancer cell genomes.

Based on this rationale, we designed preclinical trials in xenograft mice implanted with either of the two independent metastatic breast cancer cell lines, MDA231-LM2 and CN34-LM1. The mice were treated with a combination of AC chemotherapy and CXCR2 antagonist starting after lung metastasis was detectable by bioluminescence imaging (BLI) (data not shown). Tumor-bearing mice treated with AC chemotherapy alone showed a reduction in tumor growth (Figures 7A and 7B, S7A, and S7B). However, metastatic cells were not completely eliminated and micrometastases were detected throughout the lungs (Figures 7C and 7D). As a single agent, CXCR2 inhibitor had partial to no effect depending on the model system. However, when AC was combined with the CXCR2 inhibitor, lung metastatic burden was markedly reduced and the interaction between the drugs exhibited synergism (Figures 7C and 7D). Together, these results highlight the potential of targeting the CXCL1/2-S100A8/9 axis thereby sensitizing distant metastases to standard of care chemotherapy.

DISCUSSION

A Three-Way Paracrine Axis Underlying Chemoresistance and Metastasis

The major impediments to cure advanced breast cancer are the emergence of pan-resistance to all known chemotherapy drugs and the development of widely metastatic disease, two phenomena that are closely linked clinically (Gonzalez-Angulo et al., 2007). In addressing this challenge, our work links CXCL1/2 and S100A8/9 as functional partners of a paracrine loop between breast cancer cells and $CD11b^{+}Gr1^{+}$myeloid cells that supports the survival of cancer cells facing the rigors of invading new microenvironments or the impact of chemotherapy (Figure 7E). Therapeutically targeting such common mediators of chemoresistance and distant relapse would be of interest because these are the two main clinical challenges after primary tumor resection.

The critical role of the microenvironment in tumor progression and response to therapy is being increasingly recognized (Condeelis and Pollard, 2006; Denardo et al., 2011; Gilbert and

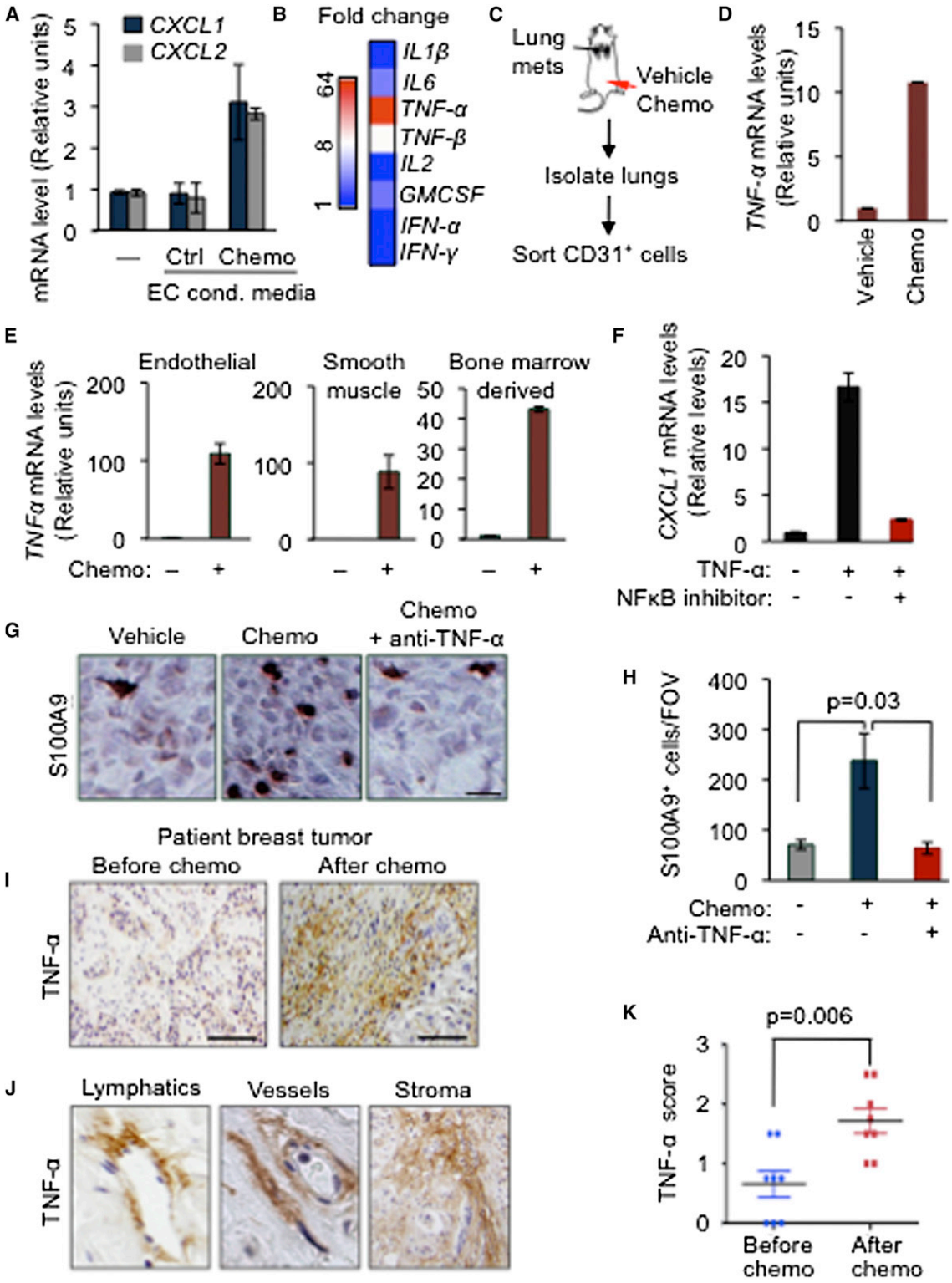

Figure 6. TNF-α from Chemotherapy-Activated Stroma Boosts the CXCL1/2 Survival Axis

(A) *CXCL1/2* expression in MDA231-LM2 cancer cells either alone (–) or in the presence of conditioned media from primary human umbilical vein endothelial cells (HUVEC) that were either untreated (control) or treated with 0.8 μM doxorubicin (chemo), as determined by qRT-PCR. Data represent average expression ± SEM. (B) Heatmap representing expression changes in inflammatory cytokines in HUVEC treated with doxorubicin (0.8 μM). Heatmap generated by conversion of qRT-PCR data that was normalized to *β2M* as housekeeping gene control.

Hemann, 2010; Shree et al., 2011; Tan et al., 2011). The present work sheds light on how the tumor microenvironment responds to chemotherapy with hyperactivation of a TNF-α-CXCL1/2-S100A8/9 paracrine axis for cancer cell survival under stress. Recent reports (Denardo et al., 2011; Gilbert and Hemann, 2010) and the present work show that chemotherapy induces a storm of cytokines and chemokines in the tumor microenvironment, many of which might be linked to chemoresistance. Our current findings suggest that this cytokine burst includes TNF-α induced in several components of the tumor microenvironment after chemotherapy treatment. An undesirable consequence of the stromal TNF-α is to further boost CXCL1/2 expression in breast cancer cells. A higher level of CXCL1/2 then drives the paracrine loop involving myeloid-cell-derived S100A8/9 to enhance cancer cell survival (Figure 7E). An adverse cycle involving TNF-α-CXCL1/2-S100A8/9 could thus be expanded in response to chemotherapy. Such a paracrine survival network could be beneficial to cancer cells under stress both in the primary tumor and at distant metastatic sites. Once initiated, this chemo-protective program could become self-sustaining, leading to the enrichment of residual aggressive clones able to resist chemotherapy and thrive in the lung parenchyma and elsewhere.

Biological and Clinical Implications

Several additional insights emerge from this work. $CD11b^+Gr1^+$ myeloid cells are a heterogeneous group with previously identified roles in tumor angiogenesis and T cell immuno-suppression (Gabrilovich and Nagaraj, 2009; Ostrand-Rosenberg and Sinha, 2009; Shojaei et al., 2007). Our study delineates a role for the $CD11b^+Gr1^+$ cells in mediating metastatic breast cancer cell survival through the production of S100A8/9. In addition to activating MAPK pathways (Gebhardt et al., 2006; Ichikawa et al., 2011), we find that S100A8/9 activate p70S6K as contributors to the prosurvival effect of S100A8/9 in these cells. In line with our findings, recent Phase 2 study in breast cancer patients showed that nonresponders of neoadjuvant chemotherapy and patients with residual disease had significantly higher circulating MDSC levels than did responders (Montero et al., 2012). These findings accentuate the clinical relevance of $CD11b^+Gr1^+$ in rendering chemotherapy ineffective and promoting metastasis.

Our findings argue that although therapy induced inflammation is a predominant feature of the use of chemotherapy, disrupting the CXCL1 driven paracrine axis could improve therapeutic response in existing lesions and also suppress metastasis, even at an advanced stage of tumor progression. CXCR2 receptor antagonists are in clinical trials for chronic inflammatory diseases (Chapman et al., 2009), and we show that these agents are a promising pharmacological approach in metastatic breast cancer when combined with standard chemotherapeutic regimen. The effective combination of chemotherapy with CXCR2 inhibitors at the metastatic site in our preclinical models underscores the potential application of this therapy to limit disseminated tumor burden. Moreover, the important role of CXCR2 in pancreatic adenocarcinoma models (Ijichi et al., 2011) and of S100A8/9 in colorectal cancer (Ichikawa et al., 2011) suggest that the relevance of targeting the CXCL1/2-S100A8/9 axis may extend beyond breast cancer.

In conclusion, our results provide mechanistic insights into the link between two major hurdles in treating breast cancer: chemoresistance and metastasis. Our findings functionally unify three important inflammatory modulators, TNF-α, CXCL1/2, and S100A8/9, in a tumor-stroma paracrine axis that provides a survival advantage to metastatic cells in stressed primary and metastatic microenvironments. This raises the possibility of clinically targeting this axis both to limit the dissemination of cancer cells and to diminish drug resistance.

EXPERIMENTAL PROCEDURES

Flow Cytometry Analysis

Whole tumors or lung tissues were dissected, cut into small pieces, and dissociated by using 0.5% collagenase Type III (Worthington Biochemical) and 1% Dispase II (Roche) in PBS for 1–2 hr. Resulting single-cell suspensions were washed in PBS with 2% heat-inactivated fetal calf serum and filtered through 70 μm nylon mesh. Cell fractions were incubated for 10 min at 4°C with anti-mouse Fc block CD16/32 antibody (2.4G2 BD) in PBS containing 1% BSA to avoid nonspecific antibody binding. Cells were subsequently washed in PBS/BSA and stained with either Ig controls or fluorophore conjugated

(C) Schematic representation of experimental procedures. Lung endothelial cells were purified from LM2 tumor-bearing mice that were treated with chemotherapy. Mice showing established lung metastasis 7 weeks after tail-vein injection of LM2 cells were either treated with vehicle (saline) or AC chemotherapy. $CD31^+$ endothelial cells were purified from dissociated lung tissue by flow cytometry.

(D) TNF-α expression in isolated $CD31^+$ lung endothelial cells from chemotherapy-treated tumor-bearing mice. n = 2–4 mice per group. Data represent averages ± SEM.

(E) *TNF-α* expression in the indicated primary cells upon doxorubicin chemotherapy treatment for 16 hr as determined by qRT-PCR analysis. Error bars represent 95% confidence interval for qRT-PCR analysis. Data are representative of three independent experiments.

(F) *CXCL1* expression in LM2 cancer cells treated with vehicle or TNF-α for 2 hr in the presence of a 100 μM NBD (NEMO binding domain) inhibitory peptide of the NF-κB pathway. Data represent averages ± SEM.

(G and H) Representative images of S100A9 expression by immunohistochemistry and quantitation of S100A9 positive cells in tumors from control or AC-chemotherapy-treated mice, with or without anti-TNF-α blocking antibody (infliximab). Mice bearing CN34LM1 tumors were treated once weekly for 5 weeks starting at 10 weeks after tumor inoculation, with PBS vehicle, AC chemotherapy (chemo), or chemotherapy plus anti-TNF-α antibody. Scale bar, 32 μm. Data are averages ± SEM; n = 3–5 mice/group. p values were calculated by Student's t test.

(I) Immunohistochemical analysis of TNF-α expression in human primary breast tumor before and after chemotherapy treatment. Scale bar, 120 μm.

(J) Stromal rich areas containing lymphatic vessels, blood vessels and fibroblasts with high TNF-α staining from primary breast tumors after AC chemotherapy treatment. Magnified fields from images taken at 40× magnification.

(K) Comparison of stromal TNF-α expression score in paired breast tumors before and after chemotherapy. n = 8 patients. p value was determined by Wilcoxon's paired test, comparing pre- and posttreatment levels from each patient.

See also Figure S6.

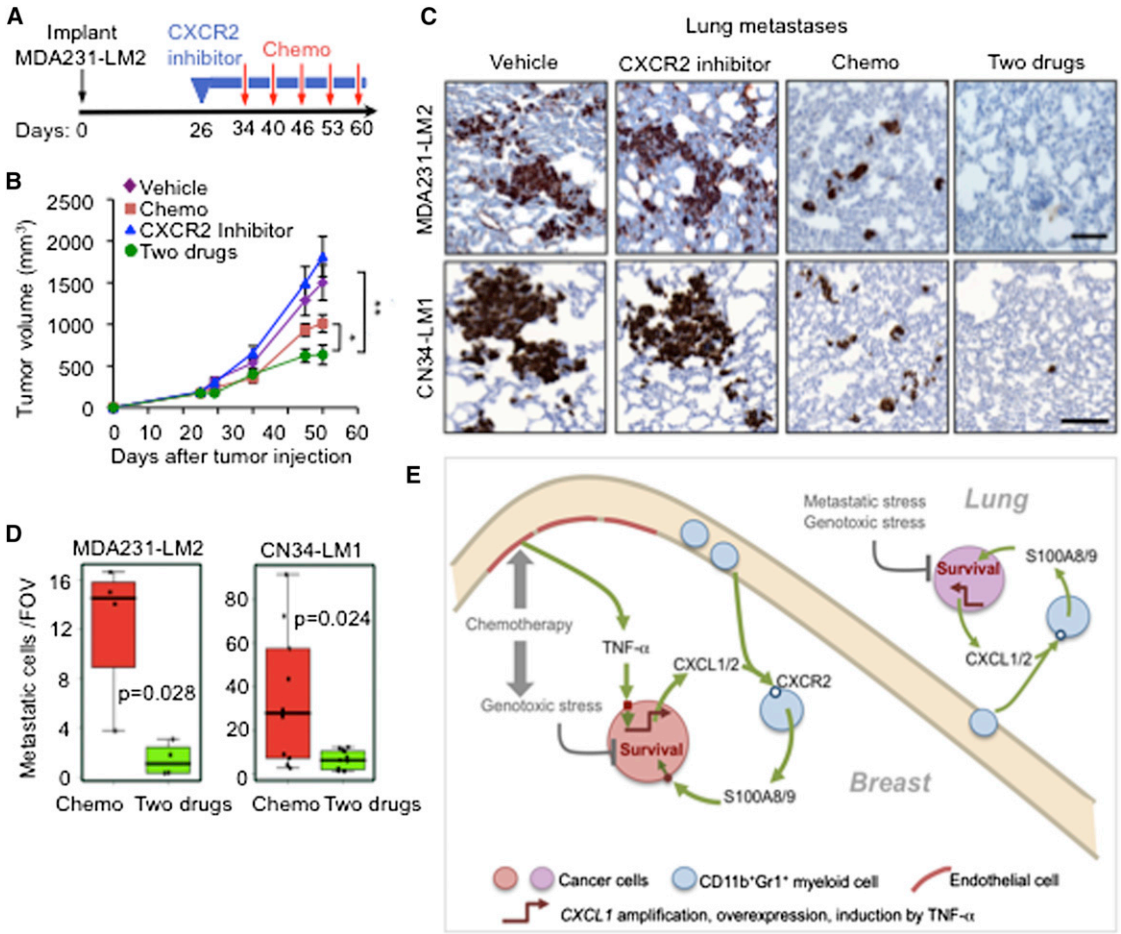

Figure 7. Pharmacological Inhibition of CXCL1 Signaling Sensitizes Cancer Cells to Chemotherapy in Metastatic Breast Cancer

(A and B) Schematic treatment flow (A), and tumor growth (B) of LM2 tumors in mice treated with PEG vehicle or CXCR2 inhibitor for the indicated periods (blue boxes) and treatment with saline vehicle or AC chemotherapy at the indicated days (red arrows). Data represent average expression ± SEM; n = 10–13 mice per group. p values were determined by Student's t test. *p = 0.02, **p = 0.007.

(C and D) Lung metastasis in MDA231-LM2 and CN34-LM1 orthotopic xenograft models undergoing treatment (C) Representative images of lung sections stained for vimentin expression marking metastatic cancer cells. Scale bars, 100 μm. (D) Quantitation of metastasis based on number of cancer cells in lung sections. Data are average foci per FOV ± SEM; n = 5–10 mice per group. Whiskers represent minimum and maximum values. p values were determined by two-tailed Wilcoxon rank-sum test.

(E) Model showing how CXCL1 paracrine interactions promote resistance to chemotherapy and metastasis in breast tumors and lung microenvironment. Genotoxic agents such as doxorubicin, cyclophosphamide, and paclitaxel limit the survival of cancer cells but also increase TNF-α production from endothelial cells. TNF-α enhances CXCL1/2 expression in cancer cells. Other modes of CXCL1/2 upregulation in cancer cells include 4q21 amplification and overexpression. CXCL1/2 from cancer cells recruit $CD11b^{+}Gr1^{+}$ myeloid cells that express CXCR2 (receptors for CXCL1/2). Myeloid cells recruited by CXCL1/2 thereby enhance viability of cancer cells through S100A8/9 factors.

See also Figure S7.

antibodies in MACS buffer (0.5% BSA, 2 mM EDTA in PBS). Data acquisition was performed on a FACS Calibur (BD Biosciences) or Cytomation CyAn (Beckman Coulter) and analysis was done by using Flowjo version 9 (Tree Star).

Animal Studies

All experiments using animals were done in accordance to a protocol approved by Memorial Sloan-Kettering Cancer Center (MSKCC) Institutional Animal Care and Use Committee (IACUC). *S100a9*$^{+/+}$ and *S100a9*$^{-/-}$mice (Hobbs et al., 2003), NOD-SCID NCR (NCI), athymic NCR nu/nu (Harlan), NIHIII homozygous nu/nu (Charles River), C57BL/6 (Jackson Labs), FVB/N (Charles River) female mice aged between 5–7 weeks were used. Autochthonous MMTV driven-polyoma virus middle T transgenic mice (Kim et al., 2009) were utilized for isolation of primary PyMT and bone-marrow-derived cells. Refer to Extended Experimental Procedures for detailed assays, drug treatment, and bone marrow transplantation.

Patient Samples

Paraffin embedded tissue microarrays containing primary breast cancer samples (IMH-364) and lymph node metastases (BRM481) were purchased from Imgenex and Pantomics, respectively. Paraffin embedded tissue microarrays and sections from lung metastases and primary breast tumor cores before and after chemotherapy treatment were acquired from the MSKCC Department of Pathology in compliance with protocols approved by the MSKCC Institutional Review Board (IRB). Staining details provided in Extended Experimental Procedures.

Bioinformatic and Statistical Analysis

All bioinformatic analyses were conducted in R. Microarray data from human tumor data sets were processed as described (Zhang et al., 2009). Survival curves for patients were calculated by using Kaplan-Meier method and differences between the curves were determined by log rank test. All other experiments were analyzed by using two-sided Wilcoxon rank-sum test or unpaired two-sided t test without unequal variance assumption unless specified. p values $\leq$ 0.05 were considered significant. See Extended Experimental Procedures for details.

SUPPLEMENTAL INFORMATION

Supplemental Information includes Extended Experimental Procedures, seven figures, and five tables and can be found with this article online at doi:10.1016/j.cell.2012.04.042.

ACKNOWLEDGMENTS

We would like to thank J. Joyce, J. Bromberg, E. Pamer, H.G. Wendel, I. Ferrero, Z. Granot, R. Downey and members of Massague laboratory for insightful discussions, J. Howard for her help with clinical cases, D. Macalinao, W. Shu, M. Akram, K. Chadalavada, T. Tong, M. Turkekul, A. Barlas, and E. de Stanchina for technical advice and support. This work was funded by NIH grants CA94060 and U54 CA163167 and the Alan and Sandra Gerry Metastasis Research Initiative. S.A. is supported by a Department of Defense Era of Hope postdoctoral fellowship. J.M. is an Investigator of the Howard Hughes Medical Institute.

Received: May 31, 2011
Revised: January 26, 2012
Accepted: April 20, 2012
Published: July 5, 2012

REFERENCES

Amiri, K.I., and Richmond, A. (2003). Fine tuning the transcriptional regulation of the CXCL1 chemokine. Prog. Nucleic Acid Res. Mol. Biol. *74*, 1–36.

Balkwill, F. (2004). Cancer and the chemokine network. Nat. Rev. Cancer *4*, 540–550.

Bergers, G., and Hanahan, D. (2008). Modes of resistance to anti-angiogenic therapy. Nat. Rev. Cancer *8*, 592–603.

Beroukhim, R., Mermel, C.H., Porter, D., Wei, G., Raychaudhuri, S., Donovan, J., Barretina, J., Boehm, J.S., Dobson, J., Urashima, M., et al. (2010). The landscape of somatic copy-number alteration across human cancers. Nature *463*, 899–905.

Bièche, I., Chavey, C., Andrieu, C., Busson, M., Vacher, S., Le Corre, L., Guinebretière, J.M., Burlinchon, S., Lidereau, R., and Lazennec, G. (2007). CXC chemokines located in the 4q21 region are up-regulated in breast cancer. Endocr. Relat. Cancer *14*, 1039–1052.

Bos, P.D., Zhang, X.H., Nadal, C., Shu, W., Gomis, R.R., Nguyen, D.X., Minn, A.J., van de Vijver, M.J., Gerald, W.L., Foekens, J.A., and Massagué, J. (2009). Genes that mediate breast cancer metastasis to the brain. Nature *459*, 1005–1009.

Cailleau, R., Young, R., Olivé, M., and Reeves, W.J., Jr. (1974). Breast tumor cell lines from pleural effusions. J. Natl. Cancer Inst. *53*, 661–674.

Chapman, R.W., Phillips, J.E., Hipkin, R.W., Curran, A.K., Lundell, D., and Fine, J.S. (2009). CXCR2 antagonists for the treatment of pulmonary disease. Pharmacol. Ther. *121*, 55–68.

Condeelis, J., and Pollard, J.W. (2006). Macrophages: obligate partners for tumor cell migration, invasion, and metastasis. Cell *124*, 263–266.

Coppé, J.P., Patil, C.K., Rodier, F., Sun, Y., Muñoz, D.P., Goldstein, J., Nelson, P.S., Desprez, P.Y., and Campisi, J. (2008). Senescence-associated secretory phenotypes reveal cell-nonautonomous functions of oncogenic RAS and the p53 tumor suppressor. PLoS Biol. *6*, 2853–2868.

Denardo, D.G., Brennan, D.J., Rexhepaj, E., Ruffell, B., Shiao, S.L., Madden, S.F., Gallagher, W.M., Wadhwani, N., Keil, S.D., Junaid, S.A., et al. (2011). Leukocyte Complexity Predicts Breast Cancer Survival and Functionally Regulates Response to Chemotherapy. Cancer Discov. *1*, 54–67.

Ebos, J.M., Lee, C.R., and Kerbel, R.S. (2009). Tumor and host-mediated pathways of resistance and disease progression in response to antiangiogenic therapy. Clin. Cancer Res. *15*, 5020–5025.

Gabrilovich, D.I., and Nagaraj, S. (2009). Myeloid-derived suppressor cells as regulators of the immune system. Nat. Rev. Immunol. *9*, 162–174.

Gebhardt, C., Németh, J., Angel, P., and Hess, J. (2006). S100A8 and S100A9 in inflammation and cancer. Biochem. Pharmacol. *72*, 1622–1631.

Gilbert, L.A., and Hemann, M.T. (2010). DNA damage-mediated induction of a chemoresistant niche. Cell *143*, 355–366.

Gonzalez-Angulo, A.M., Morales-Vasquez, F., and Hortobagyi, G.N. (2007). Overview of resistance to systemic therapy in patients with breast cancer. Adv. Exp. Med. Biol. *608*, 1–22.

Hiratsuka, S., Watanabe, A., Sakurai, Y., Akashi-Takamura, S., Ishibashi, S., Miyake, K., Shibuya, M., Akira, S., Aburatani, H., and Maru, Y. (2008). The S100A8-serum amyloid A3-TLR4 paracrine cascade establishes a pre-metastatic phase. Nat. Cell Biol. *10*, 1349–1355.

Hobbs, J.A., May, R., Tanousis, K., McNeill, E., Mathies, M., Gebhardt, C., Henderson, R., Robinson, M.J., and Hogg, N. (2003). Myeloid cell function in MRP-14 (S100A9) null mice. Mol. Cell. Biol. *23*, 2564–2576.

Hsieh, H.L., Schäfer, B.W., Sasaki, N., and Heizmann, C.W. (2003). Expression analysis of S100 proteins and RAGE in human tumors using tissue microarrays. Biochem. Biophys. Res. Commun. *307*, 375–381.

Hu, G., Chong, R.A., Yang, Q., Wei, Y., Blanco, M.A., Li, F., Reiss, M., Au, J.L., Haffty, B.G., and Kang, Y. (2009). MTDH activation by 8q22 genomic gain promotes chemoresistance and metastasis of poor-prognosis breast cancer. Cancer Cell *15*, 9–20.

Ichikawa, M., Williams, R., Wang, L., Vogl, T., and Srikrishna, G. (2011). S100A8/A9 activate key genes and pathways in colon tumor progression. Mol. Cancer Res. *9*, 133–148.

Ijichi, H., Chytil, A., Gorska, A.E., Aakre, M.E., Bierie, B., Tada, M., Mohri, D., Miyabayashi, K., Asaoka, Y., Maeda, S., et al. (2011). Inhibiting Cxcr2 disrupts tumor-stromal interactions and improves survival in a mouse model of pancreatic ductal adenocarcinoma. J. Clin. Invest. *121*, 4106–4117.

Jones, S.E. (2008). Metastatic breast cancer: the treatment challenge. Clin. Breast Cancer *8*, 224–233.

Kim, M.Y., Oskarsson, T., Acharyya, S., Nguyen, D.X., Zhang, X.H., Norton, L., and Massagué, J. (2009). Tumor self-seeding by circulating cancer cells. Cell *139*, 1315–1326.

Minn, A.J., Gupta, G.P., Siegel, P.M., Bos, P.D., Shu, W., Giri, D.D., Viale, A., Olshen, A.B., Gerald, W.L., and Massagué, J. (2005). Genes that mediate breast cancer metastasis to lung. Nature *436*, 518–524.

Minn, A.J., Gupta, G.P., Padua, D., Bos, P., Nguyen, D.X., Nuyten, D., Kreike, B., Zhang, Y., Wang, Y., Ishwaran, H., et al. (2007). Lung metastasis genes couple breast tumor size and metastatic spread. Proc. Natl. Acad. Sci. USA *104*, 6740–6745.

Montero, A.J., Diaz-Montero, C.M., Deutsch, Y.E., Hurley, J., Koniaris, L.G., Rumboldt, T., Yasir, S., Jorda, M., Garret-Mayer, E., Avisar, E., et al. (2012). Phase 2 study of neoadjuvant treatment with NOV-002 in combination with doxorubicin and cyclophosphamide followed by docetaxel in patients with HER-2 negative clinical stage II-IIIc breast cancer. Breast Cancer Res. Treat. *132*, 215–223.

Morris, P.G., McArthur, H.L., and Hudis, C.A. (2009). Therapeutic options for metastatic breast cancer. Expert Opin. Pharmacother. *10*, 967–981.

Müller, A., Homey, B., Soto, H., Ge, N., Catron, D., Buchanan, M.E., McClanahan, T., Murphy, E., Yuan, W., Wagner, S.N., et al. (2001). Involvement of chemokine receptors in breast cancer metastasis. Nature *410*, 50–56.

Murdoch, C., Muthana, M., Coffelt, S.B., and Lewis, C.E. (2008). The role of myeloid cells in the promotion of tumour angiogenesis. Nat. Rev. Cancer *8*, 618–631.

Ostrand-Rosenberg, S., and Sinha, P. (2009). Myeloid-derived suppressor cells: linking inflammation and cancer. J. Immunol. *182*, 4499–4506.

Pegram, M.D., Konecny, G.E., O'Callaghan, C., Beryt, M., Pietras, R., and Slamon, D.J. (2004). Rational combinations of trastuzumab with chemotherapeutic drugs used in the treatment of breast cancer. J. Natl. Cancer Inst. *96*, 739–749.

Poulikakos, P.I., and Rosen, N. (2011). Mutant BRAF melanomas—dependence and resistance. Cancer Cell *19*, 11–15.

Roodhart, J.M., Daenen, L.G., Stigter, E.C., Prins, H.J., Gerrits, J., Houthuijzen, J.M., Gerritsen, M.G., Schipper, H.S., Backer, M.J., van Amersfoort, M., et al. (2011). Mesenchymal stem cells induce resistance to chemotherapy through the release of platinum-induced fatty acids. Cancer Cell *20*, 370–383.

Shaked, Y., Henke, E., Roodhart, J.M., Mancuso, P., Langenberg, M.H., Colleoni, M., Daenen, L.G., Man, S., Xu, P., Emmenegger, U., et al. (2008). Rapid chemotherapy-induced acute endothelial progenitor cell mobilization: implications for antiangiogenic drugs as chemosensitizing agents. Cancer Cell *14*, 263–273.

Shojaei, F., Wu, X., Malik, A.K., Zhong, C., Baldwin, M.E., Schanz, S., Fuh, G., Gerber, H.P., and Ferrara, N. (2007). Tumor refractoriness to anti-VEGF treatment is mediated by CD11b+Gr1+ myeloid cells. Nat. Biotechnol. *25*, 911–920.

Shree, T., Olson, O.C., Elie, B.T., Kester, J.C., Garfall, A.L., Simpson, K., Bell-McGuinn, K.M., Zabor, E.C., Brogi, E., and Joyce, J.A. (2011). Macrophages and cathepsin proteases blunt chemotherapeutic response in breast cancer. Genes Dev. *25*, 2465–2479.

Stewart, T.J., and Abrams, S.I. (2007). Altered immune function during long-term host-tumor interactions can be modulated to retard autochthonous neoplastic growth. J. Immunol. *179*, 2851–2859.

Tan, W., Zhang, W., Strasner, A., Grivennikov, S., Cheng, J.Q., Hoffman, R.M., and Karin, M. (2011). Tumour-infiltrating regulatory T cells stimulate mammary cancer metastasis through RANKL-RANK signalling. Nature *470*, 548–553.

Tavazoie, S.F., Alarcón, C., Oskarsson, T., Padua, D., Wang, Q., Bos, P.D., Gerald, W.L., and Massagué, J. (2008). Endogenous human microRNAs that suppress breast cancer metastasis. Nature *451*, 147–152.

Tsai, S., and Collins, S.J. (1993). A dominant negative retinoic acid receptor blocks neutrophil differentiation at the promyelocyte stage. Proc. Natl. Acad. Sci. USA *90*, 7153–7157.

Vogl, T., Tenbrock, K., Ludwig, S., Leukert, N., Ehrhardt, C., van Zoelen, M.A., Nacken, W., Foell, D., van der Poll, T., Sorg, C., and Roth, J. (2007). Mrp8 and Mrp14 are endogenous activators of Toll-like receptor 4, promoting lethal, endotoxin-induced shock. Nat. Med. *13*, 1042–1049.

Weiss, L. (2000). Metastasis of cancer: a conceptual history from antiquity to the 1990s. Cancer Metastasis Rev. *19*, I–XI, 193–383.

Zhang, X.H., Wang, Q., Gerald, W., Hudis, C.A., Norton, L., Smid, M., Foekens, J.A., and Massagué, J. (2009). Latent bone metastasis in breast cancer tied to Src-dependent survival signals. Cancer Cell *16*, 67–78.

EXTENDED EXPERIMENTAL PROCEDURES

Cell Culture and In Vitro Treatments

MDA231-LM2, 293T, and PyMT cells were grown in DME media supplemented with 10% fetal bovine serum (FBS), 2mM L-Glutamine, 100IU/mL penicillin, 100 μg/mL streptomycin and 1 μg/mL amphotericin B. All primary bone-marrow-derived cells, including purified $CD11b^{+}Gr1^{+}$ cells, were maintained in RPMI media supplemented with 10% heat-inactivated fetal bovine serum (FBS), 2mM L-Glutamine, 100IU/mL penicillin, 100 μg/mL streptomycin and 1 μg/mL amphotericin B during coculture. The CN34-LM1 cell line was maintained in M199 media containing 2.5% FBS, 10 μg/mL insulin, 0.5 μg/mL hydrocortisone, 20ng/mL EGF, 100ng/mL cholera toxin, 0.5 μg/mL amphotericin B, 2mM L-Glutamine, 100IU/mL penicillin and 100 μg/mL streptomycin. Retroviral packaging cell line GPG29 was maintained in DME media with 2mM L-Glutamine, 50IU/mL penicillin, 50 μg/mL streptomycin, 20ng/mL doxycycline, 2 μg/mL puromycin and 0.3mg/mL G418. Primary HUVEC, (human umbilical vein endothelial cells), HBSMC (Human bronchial smooth muscle cells) were purchased from ScienCell, MPRO and U937 were purchased from ATCC and grown following manufacturer's instructions. Recombinant TNF-α and NBD (NEMO binding domain inhibitory peptide) were purchased from Roche and Imgenex, respectively, and reconstituted following manufacturer's instructions. Recombinant human CXCL1, CXCL2 and mouse Cxcl1/KC, Cxcl2/MIP-2 were purchased from R&D Systems. Coculture of cancer and tumor microenvironment cells (bone-marrow-derived cells, purified myeloid precursors or HUVEC) was for done for a period of 12-16h prior to initiating all treatments. Incubation with conditioned media or admixture of cells during treatment was done for 2h and 4h, respectively. For experiments involving recombinant S100A8/9, MDA231-LM2 cells pretreated with S100A8/9 (Calprotectin) from Hycult Biotech for 1 hr, were treated with either Doxorubicin (Sigma) at 0.8 μM alone or in combination with p38 inhibitor (SB 203580 from Cell Signaling) at 5 μM, S6K inhibitor (PF4708671) at 10 μM or Erk1/2 inhibitor (FR180204) at 10 μM for 16 hr. Cells were washed with PBS, fixed in 4% PFA for 1 hr and TUNEL assay was performed by using In situ Cell Death Detection kit, TMR Red (Roche) following manufacturer's instructions.

Generation of CXCL1/2 Knockdown Cells and S100A8/9 rescue Cells

CXCL1/2 genes were knocked down by using custom designed retroviral pSuperRetro based constructs or pLKO.1 lentiviral vectors expressing short hairpins targeting the gene products using TRCN0000057940, TRCN0000057873, TRCN0000372017 from Sigma/Open Biosystems. CXCL3 was knocked down by using human GIPZ lentiviral shRNAmir target gene set (Open Biosystems) using V2 LHS_223799 and V2 LHS_114275. *CXCL5* and *S100a8/9* were knocked down by using pLKO.1 lentiviral vectors expressing shRNA against the gene products using TRCN0000057882, TRCN0000057936, TRCN0000104758, TRCN0000072046, respectively obtained from Open Biosystems. Lentiviral particles were used to infect subconfluent cell cultures overnight in the presence of 8 μg/mL polybrene (Sigma-Aldrich). Selection of viral infected cells expressing the shRNA was done by using 2 μg/mL puromycin (Sigma-Aldrich) in the media. To generate S10a8/a9 rescue cells, *S100a8* and *S100a9* was amplified by PCR from 2 complete cDNA clones from Open Biosystems and ATCC, respectively and subcloned into pBabe-hygromycin retroviral vector via Eco R1 and Sal1 restriction sites for *S100a8* and BamH1 and Sal1 restriction sites for *S100a9*. To generate S100a8/a9 rescue cells, the following PCR primers were used to amplify S100a8 and S100a9. For *S100a8*: Forward, 5′-CAG AAT TCA TGC CGT AAC TGG A-3′ and reverse, 5′-CCA GTC GAC CTA CTC CTT GTG GCT GTC TTT GT-3′. PCR primers for *S100a9*: Forward, 5′-TAA GGA TCC ATG ACT TGC AAA ATG TCG CAG C-3′. Reverse, 5′-TAA TGT CGA CTT AGG GGG TGC CCT CCC C-3′. Retroviral particles were packed by using GPG29 packaging cell line transfected with retroviral constructs. Transfection reagent used was Lipofectamine 2000 (Invitrogen). Selection for S100A8/9-expressing cells was done by using 500 μg/mL hygromycin (Calbiochem) in media.

Cytogenetics

FISH analysis was performed as previously described (Leversha, 2001). TMA slides with patient breast cancer samples (IMH-364) and lymph node metastases (BRM481) utilized for FISH analysis were purchased from Imgenex and Pantomics, respectively. Basic clinical information and H&E are available on the manufacturer's website. FISH analysis on both cells and tissues were performed at the MSKCC Molecular Cytogenetics Core Facility by using BAC clones RP11-957J23 spanning *CXCL1* locus, and RP11-1103A22 spanning *CXCL2* locus. Briefly, RP11-957J23 was labeled by nick translation with Green dUTP and RP11-1103A22 was labeled with Red dUTP (Enzo Life Sciences, Inc., supplied by Abbott Molecular Inc.). A chromosome 4q centromeric BAC, RP11-365A22 labeled with Orange dUTP was included for reference. 10 DAPI-banded metaphases and at least 10 interphase nuclei were imaged per sample. For tissue sections, both *CXCL2* BACs were labeled with red-dUTP and the reference probe was augmented with BAC clone RP11-779E21. For image clarity, the orange reference probe was displayed as green. All FISH signals are captured by using a monochrome camera and images were pseudocolored for display. For FISH analysis detecting X and Y chromosomes, repetitive probes for mouse X and Y chromosomes were made from plasmid DXWas70 labeled with Red dUTP and BAC clone CT7-590P11 (Y heterochromatin purchased from Invitrogen) labeled with Green dUTP (Abbott Molecular). 500 cells per slide were scored for each sample independently by two members of the Molecular Cytogenetics Core Facility.

Gene Expression Analysis

Whole RNA was isolated from cells by using PrepEase RNA spin kit (USB); 100–500ng RNA was used to generate cDNA by using Transcriptor First Strand cDNA synthesis kit (Roche). Gene expression was analyzed by using Taqman gene expression assays

(Applied Biosystems). For quantitative RT-PCR, the following Taqman assays (Applied Biosystems) were used. For human genes: *CXCL1* (Hs 00236937-m1), *CXCL2* (Hs00236966_m1), *CXCL3* (Hs00171061_m1), *CXCL5* (Hs00171085_m1), *EGFL6* (Hs00170955_m1), *CCL2* (Hs00124140_m1), *CCL18* (Hs00268113_m1), *CCL20* (Hs01011368_m1), *EGFR* (Hs01076078_m1), *IL1β* (Hs01555410_m1), *IL6* (Hs00985639_m1), *TNF-α* (Hs00174128_m1), *TNFβ* (Hs00236874_m1), *IL2* (Hs00174114_m1), *GMCSF* (Hs00929873_m1), *IFNα1* (Hs00256882_s1), *IFNγ* (Hs00989291_m1). Assays used for the mouse genes: *Ccl2* (Mm00441242_m1), *Ccl20* (Mm01268754_m1), *Cxcl5* (Mm00436451_g1), *Cxcl3* (Mm01701838_m1), *S100a8* (Mm00496696_g1), *S100a9* (Mm00656925_m1), *Egfl6* (Mm00469452_m1), *Egfr* (Mm00433023_m1), *Cxcr1* (Mm00731329_s1), *Cxcr2* (Mm00438258_m1). Relative gene expression was normalized to the "housekeeping" genes *β2M* (Hs99999907_m1) and *β-actin* (Mm02619580_g1). Quantitative PCR reaction was performed on ABI 7900HT Fast Real-Time PCR system and analyzed by using the software SDS2.2.2 (Applied Biosystems). Statistical analysis was performed by using Graphpad Prism 5 software.

Immunoblotting

Cell pellets were lysed with RIPA buffer and protein concentrations determined by BSA Protein Assay Kit (Biorad). Proteins were subsequently separated by SDS-PAGE and transferred to nitrocellulose membranes. Membranes were immunoblotted with the following antibodies: Goat polyclonal antibodies from Santacruz namely S100A8 (M-19), S100A9 (M-19) used at 1:500, mouse monoclonal from Sigma against α-tubulin (clone B-5-1-2) used at 1:5000, rabbit polyclonal phospho-p65 (Ser 536), Phospho-Akt (Ser473) Clone D9E, rabbit polyclonal Phospho-Erk1/2 (Thr202/Tyr 204), rabbit polyclonal phospho-p38 (Thr180/Tyr182), rabbit Phospho-p70S6K (Thr389) Clone 108D2, rabbit polyclonal Phospho-p70S6K (Thr421/Ser424), rabbit Phospho-p70S6 (Ser235/236) Clone D57.2.2E, rabbit total p70S6 kinase Clone 49D7 all from Cell Signaling and used at 1:1000, rabbit polyclonal from Santacruz against IκBα (C-21) used at 1:500.

Phosphoprotein Array Profiling

For analysis of phosphorylation profiles of kinases, LM2 metastatic breast cancer cells were treated with recombinant human S100A8/9 for 3hrs. Cells were subsequently lysed in NP-40 lysis buffer(10mM Tris pH7.4, 150mM NaCl, 4mM EDTA, 1% NP-40, 1mM sodium vanadate, 10mM sodium fluoride, with protease inhibitors). Lysates were probed by using the human phosphokinase array blot (R&D Systems; Catalog number ARY003) according to manufacturer's instructions.

Magnetic Sorting and Flow Cytometry Analysis

$CD11b^+Gr1^+$ cells were isolated by a combination of magnetic purification and FACS sorting from dissociated tumors. Briefly, cells were positively selected by using CD11b magnetic microbeads (Miltenyi Biotech), purity and cell number were assessed by flow cytometry by using CD11b-APC following manufacturer's instructions. Eluted cell fractions were incubated for 10 min at 4°C with anti-mouse Fc block CD16/32 antibody (2.4G2 BD) in PBS containing 1% BSA. Cells were subsequently washed in PBS/BSA and stained with either Ig controls or Gr1 (Miltenyi biotech) in MACS buffer (0.5% BSA, 2 mM EDTA in PBS) following manufacturer's instructions. Cells were analyzed by flow cytometry as described before. For lung tissues, single-cell suspension was prepared and labeled with either Ig control or CD31 antibody (clone 390) from eBioscience. Cells were sorted by using FACS Aria, washed once with PBS, collected in cell lysis buffer (PrepEase Kit, USB) and frozen in −80°C for subsequent RNA isolation. For flow cytometric analysis on blood, mice were bled from the tail and processed as described previously (Sinha et al., 2008). For flow cytometric analysis of CXCR1 and 2 receptors on cancer cells, cells were incubated with mouse monoclonal antibodies against CXCR1 (clone 42705) and CXCR2 (clone 48311) from R&D Systems by using manufacturer's recommendations.

For fresh isolation of $CD11b^+Gr1^+$ cells from bone marrow for tumor coculture, cells were magnetically sorted for CD11b and Ly-6G double-positive fractions following manufacturer's instructions (Miltenyi Biotech). In brief, bone marrow cells were labeled with CD11b-PE (Miltenyi Biotech.) and magnetically sorted by using Anti-PE multisort microbeads. Positively labeled $CD11b^+$ cells were incubated with multisort release reagent followed by multisort stop reagent. Cells were subsequently labeled with Anti-Ly-6G-biotin and Anti-Biotin microbeads and magnetically labeled $CD11b^+Ly\text{-}6G^+$ fractions were eluted. Cells were plated in RPMI media supplemented with 10% heat-inactivated fetal bovine serum (FBS).

For flow cytometry analysis, the following antibodies were used: Anti-mouse antibodies from eBioscience were Ly6C Clone HK1.4, CD34 Clone RAM34, CD80 (B7-1) Clone 16-10A1, CD86 (B7-2) Clone GL1, γδ TCR Clone GL3, CD3 Clone 17A2, CD31 Clone 390, CD25 Clone PC61.5, CD8α Clone 53-6.7, CD49b Clone DX5, F4/80 Clone BM8, Anti-mouse/human CD45R/B220 Clone RA3-6B2; anti-mouse antibodies from R&D Systems were goat polyclonal IL4Rα, VEGF R1 Clone 141522; anti-mouse antibodies from BD Biosciences were CD45 Clone 30-F11, Ly6G Clone 1A8, CD4 Clone GK1.5, Sca1 Clone D7, CD117 Clone 2B8; Rat monoclonal antibodies from Miltenyi Biotech were CD11b Clone M1/70.15.11.5 that recognizes both human and mouse CD11b antigen and anti-mouse Gr1 Clone RB6-8C5.

Mice

For Orthotopic metastasis Assay, either PyMT, MDA231-LM2 or CN34LM1 cells were injected bilaterally into the 4^{th} mammary fat pad of anesthetized mice (ketamine 100mg/kg/xylazine 10mg/kg). 500,000 cells were injected in 50 μl volume PBS/matrigel mix (1:1). Matrigel used was growth factor reduced (BD Biosciences). Mammary tumor growth was monitored and growth was measured weekly by using a digital caliper. After 6 weeks, mice were sacrificed and metastasis determined in lungs by ex vivo imaging. In the

case of sized matched experiments, tumors in mammary glands were size-matched to a volume of 200 mm^3 and lung tissue was harvested for quantitation of metastasis. Lung colonization assays were performed by injecting 200,000 MDA231-LM2 (suspended in 100 μl PBS) into the lateral tail vein. Lung colonization was studied and determined by in-vivo BLI. Anesthetized mice (ketamine/xylazine) were injected retro-orbitally with D-Luciferin (150mg/kg) and imaged with IVIS Spectrum Xenogen machine (Caliper Life Sciences). Bioluminescence analysis was performed by using Living Image software, version 2.50.

Drug Treatments

For experiments involving CXCR2 inhibitor, NOD/SCID or athymic mice were injected intraperitoneally with either PEG400 (vehicle) or with SB-265610 (CXCR2 antagonist) purchased from Tocris at a dose of 2mg/kg body weight for five days a week administered once daily. For all experiments involving chemotherapy treatment, mice were injected once a week with either PBS vehicle, a combination of doxorubicin hydrochloride (Sigma) and cyclophosphamide monohydrate (Sigma) at a dose of 2mg/kg body wt and 60mg/kg body wt, respectively or Paclitaxel (Hospira) at a dose of 20mg/kg body wt or 5-Fluorouracil (APP Pharmaceuticals) at 30 mg/kg body wt for the duration indicated in the regimen. For experiments involving treatment with chemotherapy and CXCR2 antagonist, lungs were collected between 9 and 12 weeks for MDA-231-LM2 and CN34LM1 and processed for histological analysis. For experiments involving antibody against TNF-α (Infliximab from Janssen Biotech, Inc.), mice bearing CN34LM1 tumors were treated once a week intraperitoneally starting at 10 weeks post tumor inoculation and continued for 5 weeks until endpoint with the following regimen. Treatments included either PBS vehicle, a combination of doxorubicin hydrochloride (Sigma) and cyclophosphamide monohydrate (Sigma) at a dose of 2mg/kg body wt and 60mg/kg body wt either with or without anti-TNF-α blocking antibody (Infliximab) at a dose of 10mg/kg body wt.

Bone Marrow Transplantation

Bone marrow cells were harvested from male donor *S100a9*$^{+/+}$ and *S100a9*$^{-/-}$mice and transplanted into irradiated female recipient NIHIII (B, T and NK cell deficient) mice. After successful engrafting, mice were injected with LM2 cancer cells in orthotopic metastasis assay. Bone marrow was harvested by flushing femurs with sterile PBS containing penicillin/streptomycin/fungizone. Cells were washed 2X with sterile HBSS, dissociated with 18 g needles and filtered through 70 μm nylon mesh. For transplantation experiments, $2X10^6$ of the freshly isolated bone marrow cells from male donor mice were injected via tail vein into irradiated female recipient NIHIII (B, T and NK cell deficient) mice. Radiation dose used was a total of 9 Gy in two split doses. Sulfatrim antibiotics were added to food following the transplant procedure. Immune reconstitution was assessed from blood smears by X and Y FISH analysis as described in the Cytogenetics section.

Histological Staining

Tissues were fixed overnight at 4°C in 4% paraformaldehyde for mouse tissues and in 10% formalin for human tissues, paraffin-embedded and sectioned. 5 μm thick tissue sections were baked at 56°C for 1 hr, de-paraffinized and treated with 1% hydrogen peroxide for 10 min. For staining, antigen retrieval was performed either in citrate buffer (pH 6.0) or in alkaline buffer (pH 9.0) from Vector labs. Sections were incubated with a blocking buffer (MOM kit, Vector Laboratories) followed by primary antibody of interest. Corresponding biotinylated secondary antibodies and ABC avidin-biotin-DAB detection kit (all from Vector laboratories) were used for detection and visualization of staining following manufacturer's instructions. Sections were subsequently counterstained with Hematoxylin and analyzed under Zeiss Axio2Imaging microscope.

For clinical samples, TMA slides were baked for 1h at 56°C and immunostained for S100A8/9 TNF-α and Fascin (Zhang et al., 2008) expression following procedures as described. Total immunoreactivity of both stainings were evaluated and scored by a clinical pathologist (E.B) in a blinded fashion.

For immunohistochemistry, the following antibodies were used: Vimentin (Clone V9) (Vector laboratories), Rabbit polyclonal Cleaved caspase 3 Asp175(Cell Signaling), Rabbit polyclonal Von Willebrand Factor (Millipore), Rat monoclonal MECA-32 (Developmental Hybridoma Bank, Iowa), CD34 clone RAM34 (Ebioscience), phosphohistone H3 Clone 6570 (Upstate), Rat monoclonal TER-119 (BD PharMingen), Fascin Clone 55K2 (Millipore), S100A8/9 or Calgranulin clone MAC387 mouse monoclonal (Dako) for human tissues, S100A9 (M-19) goat polyclonal antibody (Santacruz) for mouse tissues, anti-mouse and anti-human TNF-α rabbit polyclonal antibodies (Rockland), rabbit polyclonal LTBP1 Atlas Ab2 (Sigma), Goat polyclonal anti-human CXCL1, C-15 (Santacruz). Vimentin,cleaved caspase 3, CD34, phosphohistone H3, immunohistochemistry were performed by the MSKCC Molecular Cytology Core Facility by using standardized automated protocols. For senescence-associated β-galactosidase staining, unfixed cryosections were stained following manufacturer's protocol (Cell Signaling).

Morphometric Analysis

Tumor vessel characteristics and lung metastatic foci size and number were quantified by using Metamorph software (Molecular Devices) as previously described (DeNardo et al., 2009; Gupta et al., 2007). In brief, 10 random images at 20X magnification were taken per tumor section stained with CD34, MECA32 or Von Willebrand factor by immunohistochemistry. A standard threshold was set on images, stained area was calculated by counting objects per field and vessel characteristics were analyzed by using Metamorph measurement module. For quantitating lung metastatic foci area and number, 8-12 random images at 20X magnification were taken per lung section stained with vimentin by immunohistochemistry. A minimum of 5 sections was analyzed per animal

across different depths of the tissue. For quantitation, a standard threshold was set to the images and the number of metastatic foci was determined. Metastatic foci were considered if they contained more than 5 cells. Foci were counted and analyzed by using Metamorph measurement module.

Immunofluorescence and TUNEL Staining

Tissues were fixed in 4% paraformaldehyde at 4°C overnight. After PBS washes, tissues were mounted and frozen in OCT compound (VWR) and stored at −80°C. 8 μm thick cryosections were used for TUNEL assays with In Situ Cell Death Detection kit, TMR Red (Roche) following manufacturer's instructions. For immunofluorescence, cryosections were incubated with a blocking buffer (Mouse on mouse- MOM kit, Vector Laboratories) followed by overnight incubation with the primary antibody of interest at 4°C in diluent (MOM kit, Vector Laboratories). Sections were incubated at room temperature for 30 min with the corresponding fluorochrome conjugated secondary antibodies (Molecular Probes). Species matched isotype antibodies were used as negative controls. Slides were mounted in aqueous mounting media containing DAPI (Fluorogel II from Electron Microscopy Sciences). Stained tissue sections were visualized under a Carl Zeiss Axioimager Z1 microscope. For immunofluorescence, the following antibodies were used: rat anti-mouse CD68 (clone FA-11) from AbD Serotec, mouse anti-human alpha smooth muscle actin (clone 1A4) from Dako, rat anti-mouse CD11b (Clone M1/70) from BD PharMingen.

Bioinformatic and Statistical Analysis

The microarray data from cell lines (GSE2603) were processed with GCRMA together with updated probe set definitions by using R packages *affy*, *gcrma* and *hs133ahsentrezgcdf* (version 10). Correlation between *CXCL1* (probe set 204470_at) and other genes was measured as the mean of Pearson's correlation coefficients from three independent microarray data sets of primary breast cancer: MSK/EMC368 (GSE2603) and (GSE2034 (Wang et al., 2005)), EMC189 (GSE5327), and EMC58 (GSE12276). Genes with extracellular function were selected by filtering out genes that did not belong to the Gene Ontology category Extracellular Space (GO:0005615). Similar analysis was performed for metastases (GSE14020) in a cohort of 67 metastatic breast cancer samples from different sites. All heatmaps were generated by the *heatmap.2* function in the R package *gplots*. Synergy between individual pharmacological agents was assessed by comparing the observed data from a combination-treatment group to a simulated additive effect that was calculated as a product of median effects of individual drugs used as single agents. Comparison of means within groups in lung metastasis assays was analyzed by using two-tailed unpaired Student's t test. Differences in TNF-α and S100A8/9 expression in staining in patient tumors before and after chemotherapy were analyzed by using Wilcoxon paired test (two-tailed).

SUPPLEMENTAL REFERENCES

DeNardo, D.G., Barreto, J.B., Andreu, P., Vasquez, L., Tawfik, D., Kolhatkar, N., and Coussens, L.M. (2009). CD4(+) T cells regulate pulmonary metastasis of mammary carcinomas by enhancing protumor properties of macrophages. Cancer Cell *16*, 91–102.

Gupta, G.P., Nguyen, D.X., Chiang, A.C., Bos, P.D., Kim, J.Y., Nadal, C., Gomis, R.R., Manova-Todorova, K., and Massagué, J. (2007). Mediators of vascular remodelling co-opted for sequential steps in lung metastasis. Nature *446*, 765–770.

Leversha, M.A. (2001). Mapping of genomic clones by fluorescence in situ hybridization. Methods Mol. Biol. *175*, 109–127.

Sinha, P., Okoro, C., Foell, D., Freeze, H.H., Ostrand-Rosenberg, S., and Srikrishna, G. (2008). Proinflammatory S100 proteins regulate the accumulation of myeloid-derived suppressor cells. J. Immunol. *181*, 4666–4675.

Wang, Y., Klijn, J.G., Zhang, Y., Sieuwerts, A.M., Look, M.P., Yang, F., Talantov, D., Timmermans, M., Meijer-van Gelder, M.E., Yu, J., et al. (2005). Gene-expression profiles to predict distant metastasis of lymph-node-negative primary breast cancer. Lancet *365*, 671–679.

Zhang, F.R., Tao, L.H., Shen, Z.Y., Lv, Z., Xu, L.Y., and Li, E.M. (2008). Fascin expression in human embryonic, fetal, and normal adult tissue. J. Histochem. Cytochem. *56*, 193–199.

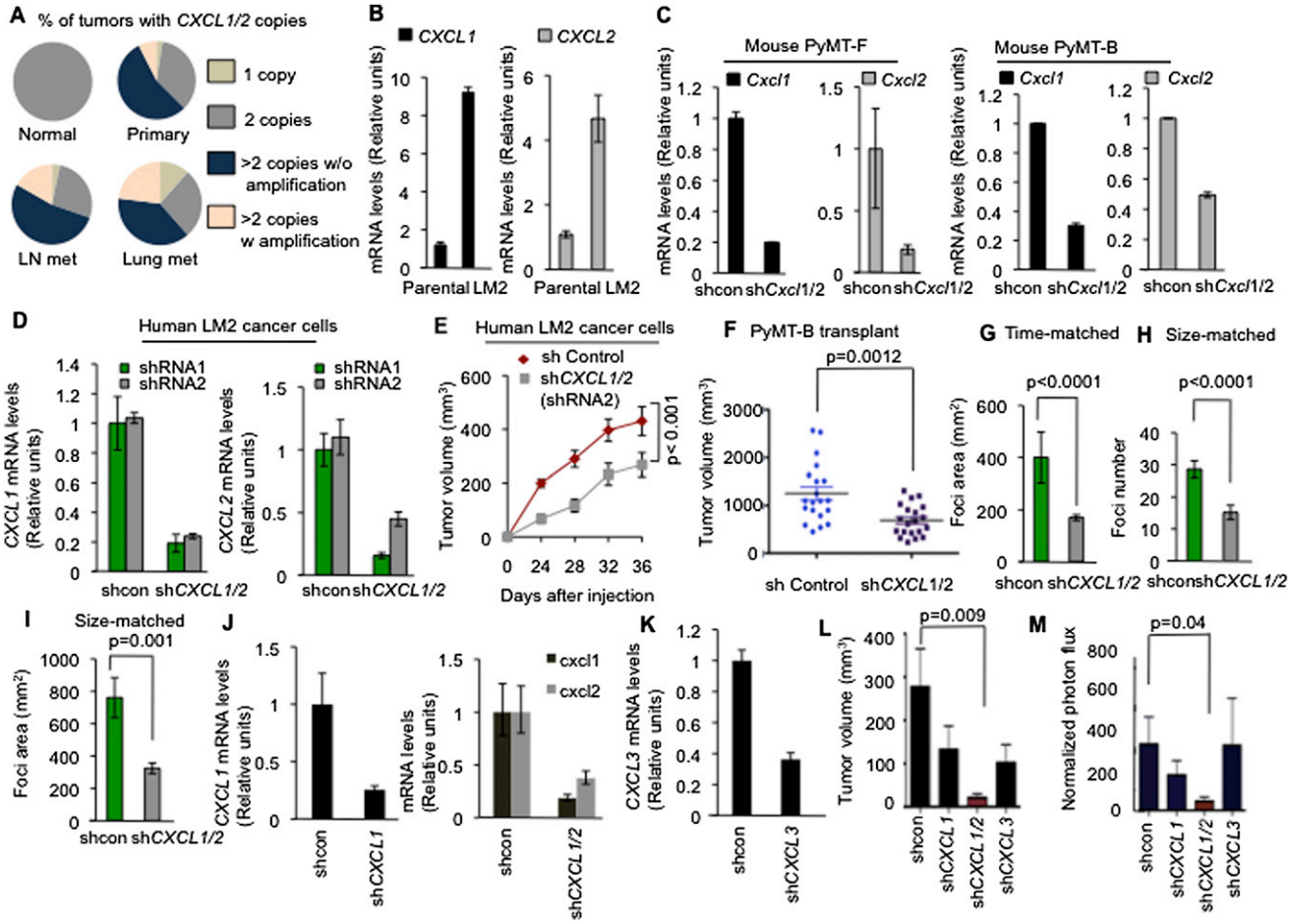

Figure S1. *CXCL1/2* in Cancer Cells Mediates Tumor Progression and Metastasis in Breast Cancer Models, Related to Figure 1.

(A) Quantification of *CXCL1/2* copies determined by FISH analysis in TMA from breast cancer patients. n = 11 (Normal), n = 40 (Primary tumors), n = 30 (Lymph node metastases, LN met), n = 26 (Lung metastases, Lung met).

(B) Expression of *CXCL1* and *CXCL2* in MDA-MB-231 breast cancer cells (parental) and lung metastatic derivative MDA231-LM2 (LM2) cells determined by qRT-PCR. Data are averages ± SEM from two independent experiments.

(C and D) *CXCL1* and *CXCL2* expression in control (sh-con) and *CXCL1/2* knockdown cells in mouse PyMT cells (C) and human LM2 cells (D). Two independent sublines of PyMT tumor cells derived from MMTV-PyMT transgenic mice in FVB/N (PyMT-F for short) and C57/BL6 backgrounds (PyMT-B for short) are shown in C. Two independent short hairpin RNAs (shRNA1 and shRNA2) targeting *CXCL1/2* tested in LM2 cells are shown in D. Expression was determined by qRT-PCR in two independent experiments. Data are average ± SEM.

(E) Mammary tumors derived from LM2 cells expressing either control or sh*CXCL1/2* in orthotopic metastasis assay (second set of hairpin). Data are shown as averages ± SEM; n = 10 per group. p values determined by Student's t test.

(F) Mammary tumor volume (mm^3) from PyMT-B-derived tumor cells expressing either control or sh*CXCL1/2* in orthotopic metastasis assay on day 19 post tumor inoculation. Data are shown as averages ± SEM; n = 20 tumors per group. p values were determined by Student's t test.

(G–I) Lung metastasis in a xenograft mouse model determined by automated counting of metastatic foci area or foci number. Metastasis was determined in mice where control and sh*CXCL1/2* LM2 tumors were time matched (G) or size matched at 200mm^3 (H-I). Data are averages ± SEM; n = 5 mice per group. p values were determined by Student's t test.

(J and K) Chemokine expression in LM2 cells transduced with (J) sh-control, sh-*CXCL1*, sh-*CXCL1/2* or (K) sh-*CXCL3* vectors. Expression was determined by qRT-PCR. Error bars represent 95% confidence interval. Data are representative of two independent experiments.

(L) Mammary tumor volume (mm^3) from LM2 cancer cells expressing either shRNA control, sh*CXCL1*, sh*CXCL1/2 or* sh*CXCL3* in orthotopic metastasis assay 5 weeks post tumor inoculation. *shcon* represent pooled tumors from mice bearing either pLKO.1 or pGIPZ vectors. Data are shown as averages ± SEM; n = 6-20 tumors. p values determined by Student's t test.

(M) BLI quantification of lung colonization ability of control, sh*CXCL1,* sh*CXCL1/2 and* sh*CXCL3* LM2 cells. Data are averages ± SEM; *shcon* represents pooled tumors from mice bearing either pLKO.1 or pGIPZ,(n = 27), sh*CXCL1* (n = 3), sh*CXCL1/2* (n = 8), sh*CXCL3* (n = 17) represents pooled tumors from mice bearing two independent hairpins targeting CXCL3 with similar knockdown levels. p values determined by Student's t test.

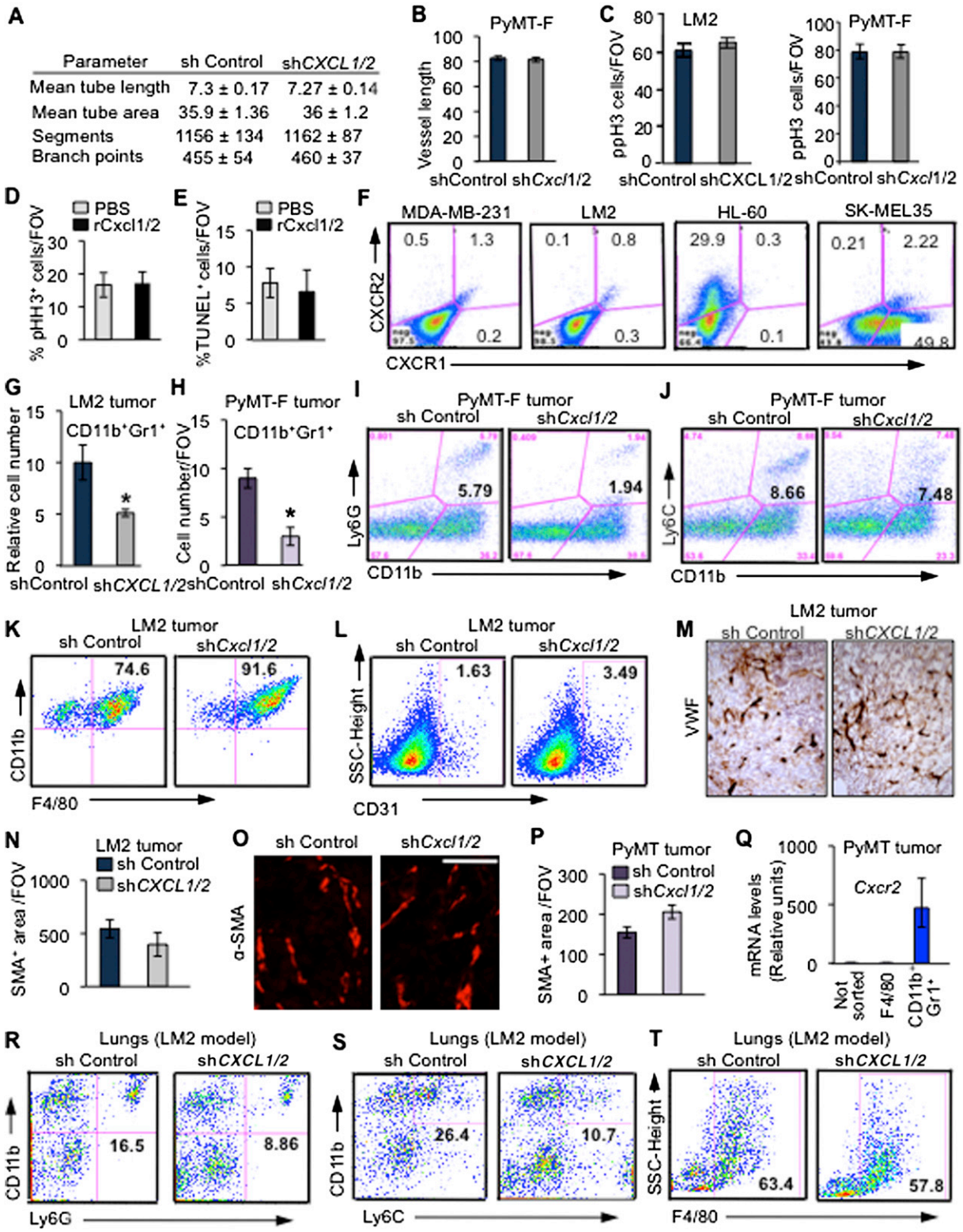
A
Parameter
sh Control
shCXCL1/2
Mean tube length
7.3 ± 0.17
7.27 ± 0.14
Mean tube area
35.9 ± 1.36
36 ± 1.2
Segments
1156 ± 134
1162 ± 87
Branch points
455 ± 54
460 ± 37
B
PyMT-F
Vessel length
shControl shCxcl1/2
C
LM2
ppH3 cells/FOV
shControl shCXCL1/2
PyMT-F
ppH3 cells/FOV
shControl shCxcl1/2
D
PBS
rCxcl1/2
% pHH3+ cells/FOV
E
PBS
rCxcl1/2
%TUNEL+ cells/FOV
F
MDA-MB-231
LM2
HL-60
SK-MEL35
CXCR2
CXCR1
0.5
1.3
0.2
0.1
0.8
0.3
29.9
0.3
0.1
0.21
2.22
49.8
G
LM2 tumor
CD11b+Gr1+
Relative cell number
shControl shCXCL1/2
H
PyMT-F tumor
CD11b+Gr1+
Cell number/FOV
shControl shCxcl1/2
I
PyMT-F tumor
sh Control
shCxcl1/2
Ly6G
CD11b
5.79
1.94
J
PyMT-F tumor
sh Control
shCxcl1/2
Ly6C
CD11b
8.66
7.48
K
LM2 tumor
sh Control
shCxcl1/2
CD11b
F4/80
74.6
91.6
L
LM2 tumor
sh Control
shCxcl1/2
SSC-Height
CD31
1.63
3.49
M
LM2 tumor
sh Control
shCXCL1/2
VWF
N
LM2 tumor
sh Control
shCXCL1/2
SMA+ area /FOV
O
sh Control
shCxcl1/2
α-SMA
P
PyMT tumor
sh Control
shCxcl1/2
SMA+ area /FOV
Q
PyMT tumor
Cxcr2
mRNA levels (Relative units)
Not sorted
F4/80
CD11b+ Gr1+
R
Lungs (LM2 model)
sh Control
shCXCL1/2
CD11b
Ly6G
16.5
8.86
S
Lungs (LM2 model)
sh Control
shCXCL1/2
CD11b
Ly6C
26.4
10.7
T
Lungs (LM2 model)
sh Control
shCXCL1/2
SSC-Height
F4/80
63.4
57.8

Figure S2. CXCL1/2 Inhibition in Cancer Cells Does Not Affect Tumor Angiogenesis or Proliferation but Affects Myeloid Recruitment, Related to Figure 2.

(A and B) Automated morphometric analysis of tumor vessels detected by immunostaining of endothelial marker CD34. Control and sh*CXCL1/2* mammary tumors (LM2, A or PyMT-F, B) were analyzed at endpoint (6 and 9 wks post tumor inoculation, respectively). Data are shown as averages ± SEM; n = 4–6 mice per group. p values determined by Student's t test.

(C) Proliferation in control and sh*CXCL1/2*- LM2 or PyMT-F mammary tumors determined by phosphohistone H3 immunostaining at endpoint (6 and 9 wks post tumor inoculation, respectively). Data are shown as average ± SEM; n = 5 mice per group. p values determined by Student's t test.

(D and E) Quantification of proliferation and apoptosis in PyMT-F tumor cells determined by phosphohistoneH3 immunostaining (D) and TUNEL staining (E), respectively upon treatment with either saline or recombinant mouse-CXCL1/2 (50 ng/ml each) for 12h. Numbers represent percentage positive cells over DAPI+ cells per FOV. Data are shown as average ± SEM from quadruplicates per condition. p values determined by Student's t test.

(F) Analysis of CXCR1 and CXCR2 receptor expression in MDA-MB-231 parental and LM2 cells by flow cytometry. SK-MEL-35 and HL60 cell lines were used as positive controls for CXCR1 and CXCR2, respectively.

(G and H) $CD11b^+Gr1^+$ cells in tumors from LM2 or PyMT-F tumor cells expressing either shRNA control or sh*CXCL1/2* were quantitated by a combination of magnetic and flow sorting in G and immunostaining analysis in H.

(I and J) Analysis of myeloid cells in tumors derived from PyMT cells transduced with either control or sh*Cxcl1/2* hairpins 5 weeks post tumor inoculation by flow cytometric analysis. For flow cytometric analysis, number in the dot plots indicate percentages of either $CD11b^+Ly6G^+$ (I) or $CD11b^+Ly6C^+$ (J) cells represented in the quadrant expressed as percentages of total $CD45^+$ leukocyte infiltrates from the same tumor. Results are representative of three independent experiments (n = 3).

(K–N) Analysis of macrophages, endothelial cells and myofibroblasts in tumors derived from LM2 cells transduced with either control or sh*CXCL1/2* hairpins 5 weeks post tumor inoculation by a combination of flow cytometric and immunostaining analysis. $CD11b^+F4/80^+$ percentages are shown out of total $CD45^+$ leukocyte infiltrates in the tumor (K). $CD31^+$ endothelial cells are quantitated by FACS analysis from the same tumors (L). Results are representative of three independent experiments (n = 3). Endothelial cells were immunostained with an antibody against Von Willebrand factor and representative stained images are shown (M). Quantitation of SMA+ myofibroblasts represented by immunostained area/FOV (N) using Metamorph. Data are shown as averages ± SEM; n = 4–6 mice per group. p values were determined by Student's t test.

(O–P) Representative images and quantitation of SMA^+ myofibroblasts represented by immunostained area/FOV in tumors derived from PyMT cells transduced with either control or sh*Cxcl1/2* hairpins are shown. Scale bar, 20 μm. Data are shown as averages ± SEM; n = 4–6 mice per group. p values were determined by Student's t test.

(Q) Expression of *Cxcr2* receptor in sorted subpopulations of MMTV-PyMT transgenic tumors determined by qRT-PCR. Error bars represent 95% confidence interval. Data are representative of two independent experiments.

(R–T) Analysis of myeloid cells 4 weeks post tumor inoculation by flow cytometry in the lungs from mice injected intravenously with LM2 cancer cells transduced with either control or sh*CXCL1/2* hairpins. For flow cytometric analysis, number in the dot plots indicate percentages of either $CD11b^+Ly6G^+$, $CD11b^+Ly6C^+$ or $F4/80^+$ myeloid cells represented in the quadrant expressed as percentages of total $CD45^+$ leukocyte infiltrates from the same tumor. Results are representative of two independent experiments.

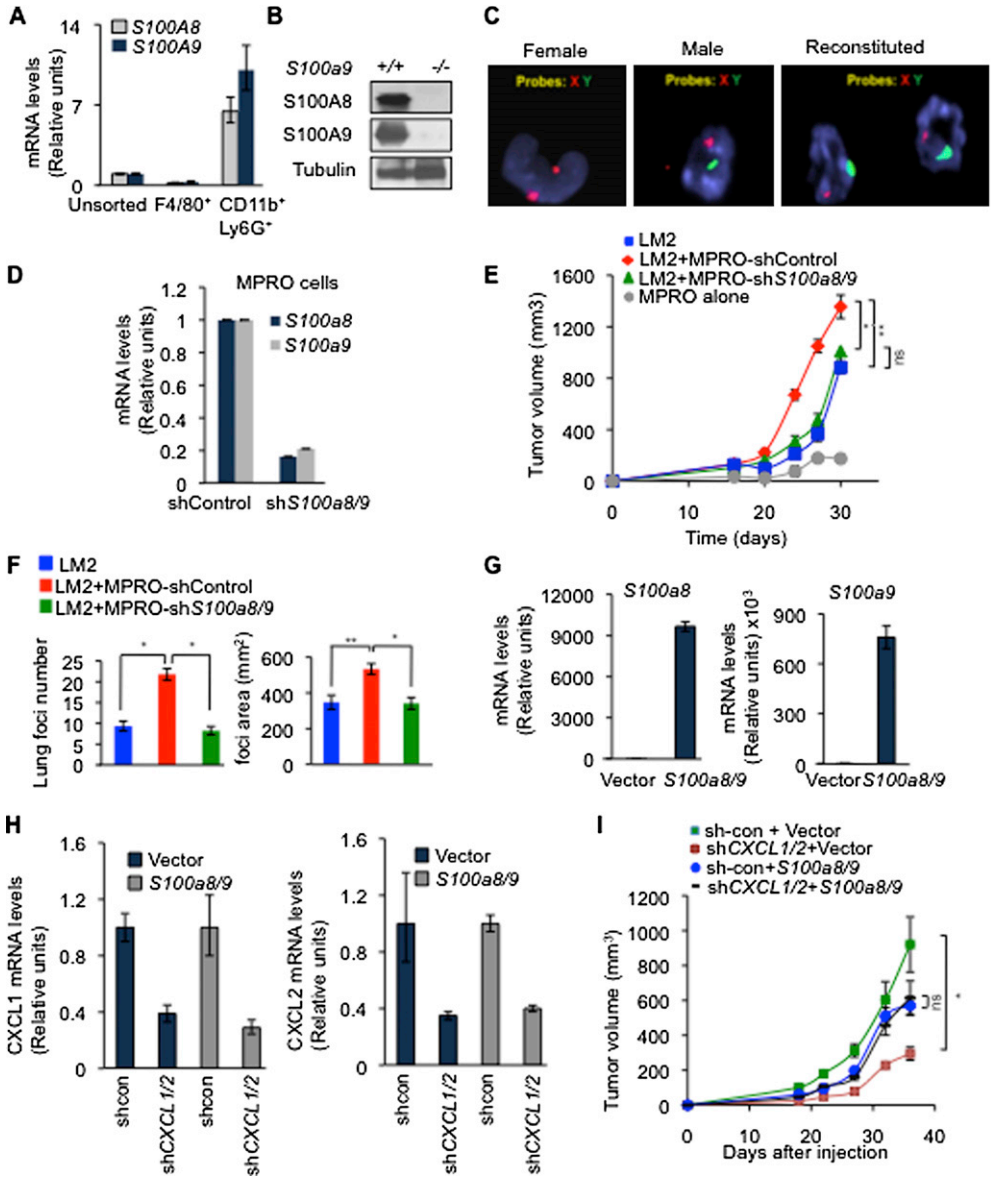

Figure S3. Ectopic S100A8/9 Expression Restores Tumor Growth and Metastasis in *CXCL1/2* Knockdowns. Related to Figure 3.

(A) Expression of *S100a8* and *S100a9* in sorted CD11b$^+$Ly6G$^+$ cells compared to unsorted tumor and F4/80$^+$ macrophages determined by qRT-PCR analysis from MMTV-PyMT autochthonous mammary cancer model. Error bars represent 95% confidence interval. Data are representative of two independent experiments.

(B) Western-blot analysis showing S100A8 and S100A9 expression in isolated bone marrow cells from *S100a9*$^{+/+}$ or *S100a9*$^{-/-}$ mice. Loading control: tubulin.

(C) Efficiency of bone marrow reconstitution. Representative images of FISH analysis using probes against X and Y chromosomes from blood smears.

(D) Expression of *S100a8/9* in control (shControl) and sh-*S100a8/a9* myeloid MPRO cell line determined by qRT-PCR in two independent experiments. Data are average ± SEM.

(E) Mammary growth curves arising from tumors from LM2 cells alone, LM2 cells coinjected with MPRO cells transduced with either control or sh*S100a8*/a9 in 1:3 ratio in the mammary fat pad. MPRO cells alone are used as a control. Tumor size was measured at the indicated times by using a digital caliper. Data are averages ± SEM. Control n = 4-12 tumors per group. p values were determined by t test. *, ** denote p = 0.02 and 0.002, respectively, ns indicates not significant.

(F) Quantitation of spontaneous lung metastasis burden from mammary tumors described in (F) after 5 weeks post tumor inoculation. Cancer cells within lungs were detected by vimentin immunostaining and metastasis was determined by automated counting of number of foci per field of view (FOV). Shown are averages ± SEM. p values were determined by t test. * indicate p value < 0.0001 except **, which indicates p value of 0.0005.

(G) Expression of *S100a8/9* in vector control and *S100a8/9* overexpressing LM2 cells determined by qRT-PCR in two independent experiments. Data are average ± SEM.

(H) Expression of *CXCL1/2* in vector control and *S100a8/a9* overexpressing LM2 cells transduced with either sh-control or hairpin targeting *CXCL1/2*. Expression was determined by qRT-PCR. Error bars represent 95% confidence interval. Data are representative of two independent experiments.

(I) Mammary tumor growth from control and sh*CXCL1/2* LM2 cells transduced with either vector control or vector expressing *S100a8/9*. Data are shown as averages ± SEM; n = 10 mice per group. p values were determined by t test. * indicate p = 0.0014 and ns indicates not significant.

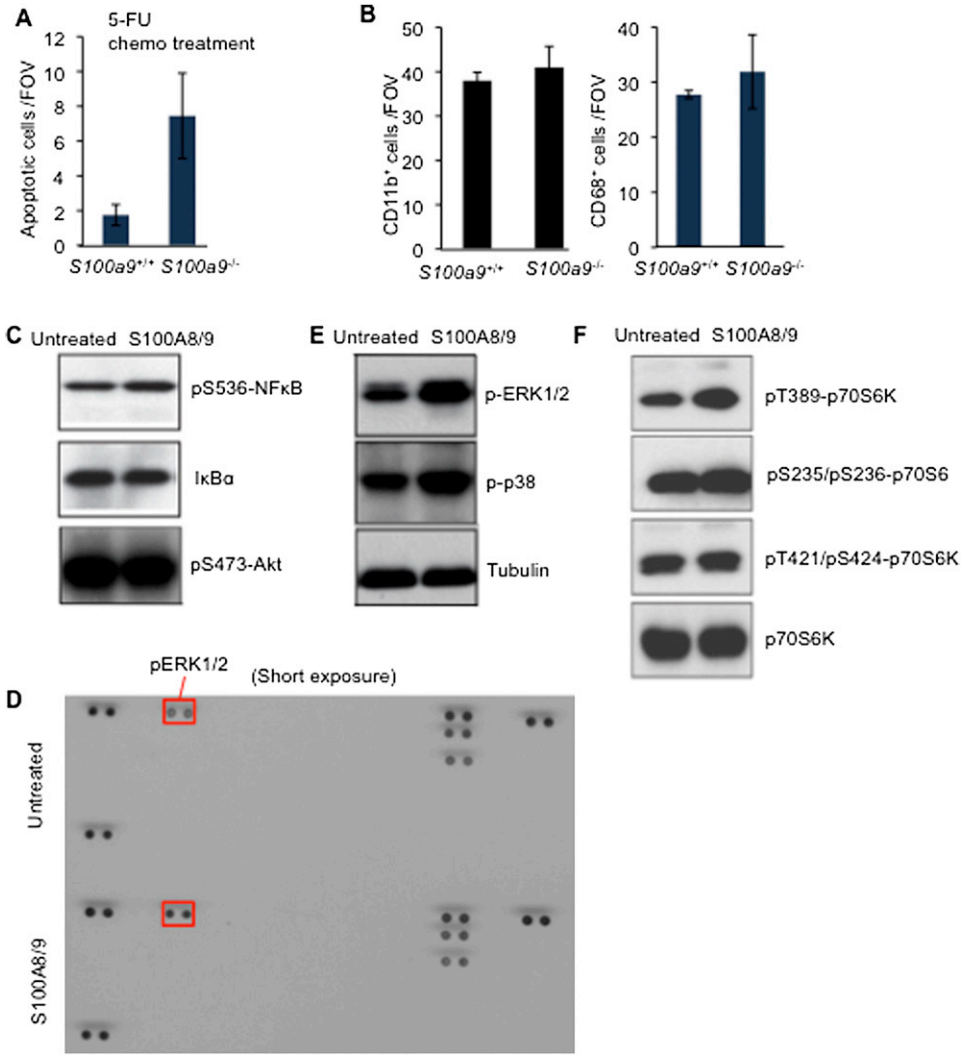

Figure S4. Prosurvival Role of S100A8/9 by Activation of ERK/p70S6K Signaling Pathways in LM2 Cancer Cells, Related to Figure 4.

(A) Quantification of apoptosis by TUNEL staining in tumor-associated areas in the lungs in mice bearing LM2 tumors transplanted with either *S100a9*$^{+/+}$or *S100a9*$^{-/-}$ bone marrow and subsequently treated with 5-FU.

(B) Immunostaining analysis of CD11b^{+} and CD68^{+} myeloid cells in the tumor-associated areas in the lung at 60 days post LM2 tumor inoculation in the mammary fat pad in mice transplanted with either *S100a9*$^{+/+}$ or *S100a9*$^{-/-}$ bone marrow. Data are shown as averages ± SEM; n = 2–4 tumors per group. p values were determined by t test.

(C) Immunoblot analysis of lysates of LM2 cells treated with either saline or 10 μg/ml S100A8/9 and probed with the indicated antibodies. Data shown are representative of three independent experiments.

(D) Screening of signaling pathways activated by S100A8/9 in LM2 metastatic cancer cells by probing human phosphokinase array with lysates from cells treated with either PBS or 10 μg/ml recombinant S100A8/9. Lower exposure is shown in this panel and higher exposure of the same blot is shown in Figure 4. Signaling proteins showing highest phosphorylation increases upon S100A8/9 treatment are highlighted on the blots.

(E and F) Immunoblot analysis of lysates of LM2 cells treated with either saline or 10 μg/ml S100A8/9 and probed with the indicated antibodies confirming the phosphokinase array profiling results. Data shown are representative of two independent experiments.

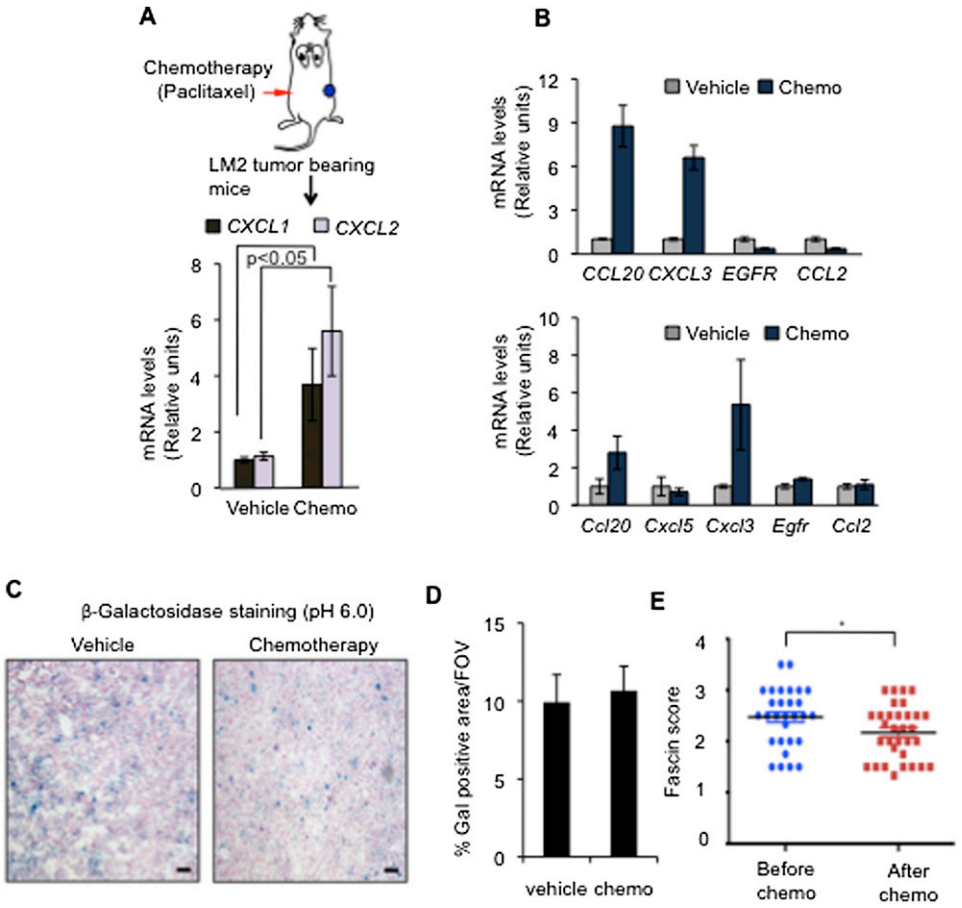

Figure S5. CXCL1 Chemokine Program Is Induced in Response to Chemotherapy, Related to Figure 5.

(A) Schematic diagram of chemotherapy treatment. *CXCL1/2* expression in mammary LM2 tumors from mice treated with paclitaxel chemotherapy weekly. Data represent average expression ± SEM; n = 5 mice per group. p value was determined by Student's t test.

(B) Gene expression analysis of *CXCL1*-associated genes shown in Table S3. Human specific primers (top panel) or mouse specific primers (bottom panel) used in qRT-PCR comparing control (vehicle) and AC-chemotherapy-treated (chemo) tumors. No detectable expression of *CXCL5*, *EGFL6, CCL18* using human primers and *Egfl6* for mouse primers. Data represent average expression ± SEM; n = 5-11 mice per group.

(C and D) Representative β-galactosidase staining (pH 6.0) for senescence and quantitation of β-galactosidase-positive cells/FOV in tumor cryosections harvested from mice treated with either saline vehicle or AC chemotherapy for two weeks from two independent cohorts of 2-3 mice per group. Scale bar represents 70 μm.

(E) Fascin expression score in paired patient tumor samples, before and after chemotherapy. Data represent expression score. n = 32 patients. * represents p = 0.01. p values determined by Wilcoxon's paired test, comparing pre and posttreatment levels from each patient.

Error bars represent SEM.

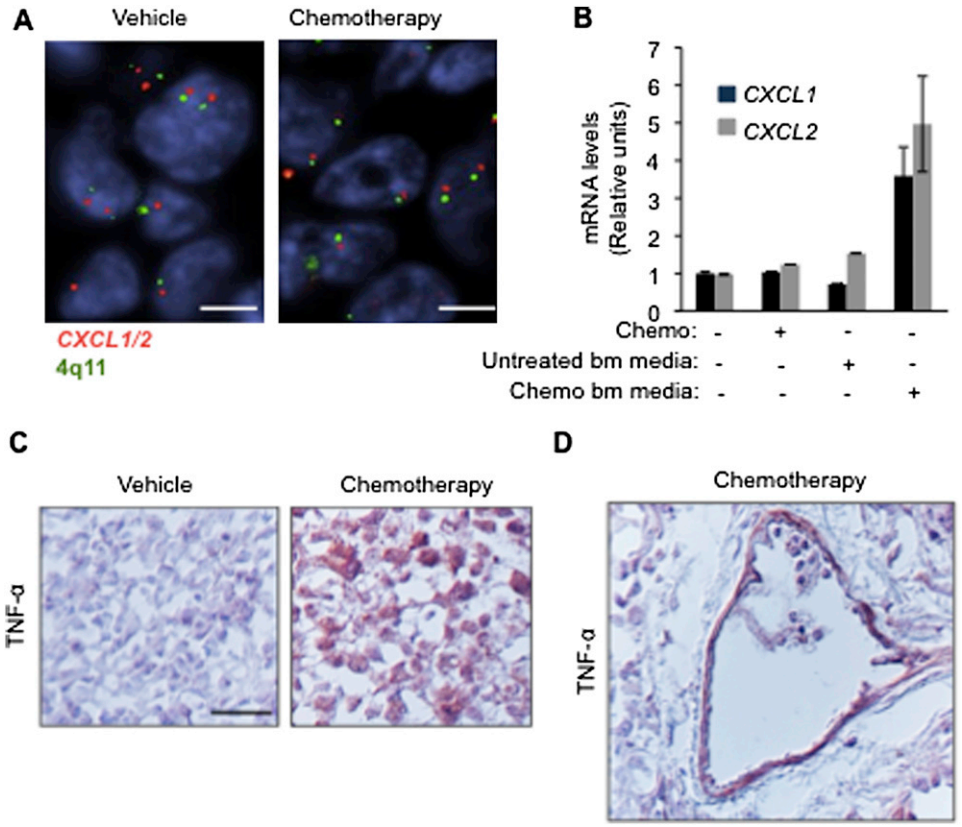

Figure S6. Chemotherapy Induces Stromal TNF-α Leading to Enhanced CXCL1/2 Expression in Cancer Cells, Related to Figure 6.

(A) *CXCL1/2* copy-number analyzed by FISH in tumors from mice bearing LM2 cancer cells and treated with saline vehicle or AC chemotherapy. Scale bar, 5 μm.

(B) *CXCL1/2* expression determined by qRT-PCR in LM2 cancer cells either alone, treated with chemotherapy or after incubation with conditioned media from saline-treated (bm-media) or doxorubicin-treated (chemo bm-media) primary mouse bone-marrow-derived cells Chemotherapy (chemo): Doxorubicin (0.8 μM). Data represent average expression ± SEM.

(C) Immunohistochemical analysis of mouse TNF-α expression in mammary breast tumor before and after AC chemotherapy treatment for 2 weeks in mice bearing LM2 tumors. Scale bar, 32 μm.

(D) Blood vessel structures with high TNF-α staining from mammary tumors post chemotherapy treatment. Magnified fields from images taken at 40X magnification.

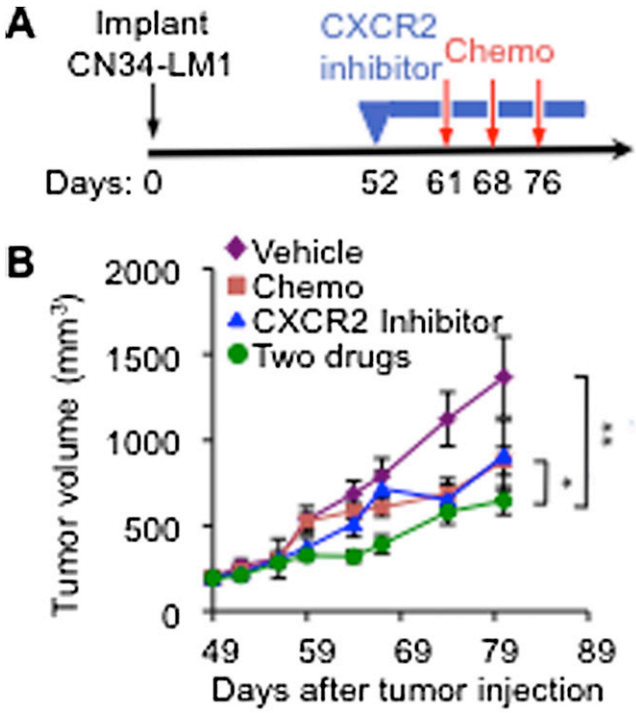

Figure S7. Pharmacological Inhibition of CXCL1-Driven Paracrine Axis Improves Chemotherapeutic Response in Metastasis Models, Related to Figure 7.

(A and B) Schematic treatment flow (A), and tumor growth (B) of CN34-LM1 tumors in mice treated with PEG vehicle or CXCR2 inhibitor for the indicated periods (blue boxes) and treatment with saline vehicle or AC chemotherapy at the indicated days (red arrows). Data represent average expression ± SEM; n = 7-11 mice per group. p values were determined by Student's t test. *p = 0.049, **p = 0.001.